Improved estimate of global gross primary production for reproducing its long-term variation, 1982-2017

Yi Zheng[1], Ruoque Shen[1], Yawen Wang[1,2], Xiangqian Li[1], Shuguang Liu[3], Shunlin Liang[4,5], Jing M. Chen[6,7], Weimin Ju[7,8], Li Zhang[9], Wenping Yuan[1,2*]

[1]School of Atmospheric Sciences, Sun Yat-sen University, Zhuhai 519082, Guangdong, China;
[2]Southern Laboratory of Ocean Science and Engineering (Guangdong, Zhuhai), Zhuhai 519000, Guangdong, China
[3]College of Life Science and Technology, Central South University of Forestry and Technology (CSUFT), Changsha, Hunan 410004, China
[4]Department of Geographical Sciences, University of Maryland, College Park, MD 20742 USA
[5]School of Remote Sensing Information Engineering, Wuhan University, Wuhan 430072, Hubei, China
[6]Department of Geography, University of Toronto, Canada, M5G 3G3
[7]International Institute for Earth System Sciences, Nanjing University, Nanjing, China.
[8]Jiangsu Center for Collaborative Innovation in Geographical Information Resource Development and Application, Nanjing, China.
[9]Key Laboratory of Digital Earth Science, Institute of Remote Sensing and Digital Earth, Chinese Academy of Sciences, Beijing 100094, China

Correspondence to: yuanwpcn@126.com (W. Yuan).

Abstract. Satellite-based models have been widely used to simulate vegetation gross primary production (GPP) at the site, regional, or global scales in recent years. However, accurately reproducing the interannual variations in GPP remains a major challenge, and the long-term changes in GPP remain highly uncertain. In this study, we generated a long-term global GPP dataset at 0.05 °latitude by 0.05 °longitude and 8-day interval by revising a light use efficiency model (i.e. EC-LUE model). In the revised EC-LUE model, we integrated the regulations of several major environmental variables: atmospheric CO_2 concentration, radiation components, and atmospheric vapor pressure deficit (VPD). These environmental variables showed substantial long-term changes, which could greatly impact the global vegetation productivity. Eddy covariance (EC) measurements at 95 towers from the FLUXNET2015 dataset, covering nine major ecosystem types around the globe, were used to calibrate and validate the model. In general, the revised EC-LUE model could effectively reproduce the spatial, seasonal, and annual variations in the tower estimated GPP at most sites. The revised EC-LUE model could explain 71% of the spatial variations in annual GPP over 95 sites. At more than 95% of the sites, the correlation coefficients (R^2) of seasonal changes between tower estimated and model simulated GPP are larger than 0.5. Particularly, the revised EC-LUE model improved the model performance in reproducing the interannual variations in GPP, and the averaged R^2 between annual mean tower estimated and model simulated GPP is 0.44 over all 55 sites with observations longer than 5-years, which is significantly higher than those of original EC-LUE model (R^2 = 0.36) and other LUE models (R^2 ranged from 0.06 to 0.30 with an average value of 0.16). At the global scale, GPP derived from light use efficiency models, machine learning models, and process-based biophysical models exist substantial differences in magnitude and interannual variations. The revised EC-LUE model quantified the mean global GPP from 1982 to 2017 as 106.2±2.9 Pg C yr^{-1} with the trend 0.15 Pg C yr^{-1}.

Sensitivity analysis indicated that GPP simulated by the revised EC-LUE model was sensitive to atmospheric CO_2 concentration, VPD, and radiation. Over the period of 1982–2017, the CO_2 fertilization effect on the global GPP (0.22 ± 0.07 Pg C yr^{-1}) could be partly offset by increased VPD (−0.17 ± 0.06 Pg C yr^{-1}). The long-term changes in environmental variables could be well reflected in global GPP. Overall, the revised EC-LUE model is able to provide a reliable long-term estimate of global GPP. The GPP dataset is available at https://doi.org/10.6084/m9.figshare.8942336 (Zheng et al., 2019).

1 Introduction

Vegetation gross primary production (GPP) is the largest carbon flux component within terrestrial ecosystems and plays an essential role in regulating the global carbon cycle (Canadell et al., 2007; Zhao et al., 2010). As a primary variable of the terrestrial ecosystem cycle, GPP estimates will substantially determine other variables of the carbon cycle (Yuan et al., 2011). Satellite-based GPP models have been developed based on the light use efficiency (LUE) principle (Monteith, 1972; Potter et al., 1993; Running et al., 2004; Xiao et al., 2005; Yuan et al., 2007). Thus far, LUE models have been a major tool for investigating the spatio-temporal changes in GPP and the environmental dominates, either independently or by combining with other ecosystem models (Keenan et al., 2016; Smith et al., 2016).

However, current LUE models exhibit poor performance in reproducing the interannual variations in GPP. A previous study indicated that seven LUE models could only explain 6–36% of the interannual variations in GPP at 51 eddy covariance (EC) towers (Yuan et al., 2014). Similarly, a model comparison showed that none of the examined 16 process-based biophysical models or the 3 remote sensing products (BESS, MODIS C5, and MODIS C5.1) could consistently reproduce the observed interannual variations in GPP at 11 forest sites in North America (Keenan et al., 2012). Seven LUE models simulated the long-term trends in global GPP varied from −0.15 to 1.09 Pg C yr^{-1} over the period 2000–2010 (Cai et al., 2014). An important reason for the poor performance in modeling the interannual variability is that the effect of environmental regulations on vegetation production is not completely integrated into the LUE models (Stocker et al., 2019). In particular, the long-term changes in several environmental variables are very important for accurately simulating the GPP series at the decadal scale.

Several environmental variables should be included in GPP models. Firstly, as we all know the rising atmospheric CO_2 concentration in the past few decades substantially stimulated global vegetation growth (Zhu et al., 2016; Liu et al., 2017). Field experiments using greenhouses or open-top chambers showed that an increase of approximately 300 ppm in CO_2 concentration can increase the photosynthesis of C3 plants on the order of 60% (Norby et al., 1999). Free-air CO_2 enrichment (FACE) experiments generally confirmed the enhancement in net primary production (NPP) with the rising CO_2 concentration (Ainsworth and Long, 2005). For example, four FACE experiments indicated that the forest NPP consistently increased at the median of 23 ± 2% when the ambient CO_2 concentration was elevated to approximately 550 ppm (Norby et al., 2005). According to observations, the atmospheric CO_2 concentration has risen by approximately 20% from 340 ppm

(1982) to 410 ppm (2018) (https://www.esrl.noaa.gov/). However, the effects of CO_2 fertilization on GPP have not been integrated in most current satellite-based LUE models.

Secondly, solar radiation, or more specifically the photosynthetic active radiation (PAR) substantially influences the vegetation production of the terrestrial ecosystem (Alton et al., 2007; Kanniah et al., 2012; Krupkova et al., 2017). Study indicated that the solar radiation incident at the earth surface underwent significant decadal variations (Wild et al., 2005). A comprehensive analysis based on the datasets of worldwide distributed sites indicated significant decreases in solar radiation (2% per decade) from the late 1950s to 1990 in the regions of Asia, Europe, North America, and Africa (Gilgen et al., 1998). A later assessment by Wild et al. (2005) showed that the radiation increased at widespread locations since the mid-1980s. However, not only the total amount of solar radiation or PAR incident at the earth surface but more importantly, their partitioning into direct and diffuse radiations, impact the vegetation productivity (Urban et al., 2007; Kanniah et al., 2012). Increased proportion of diffuse radiation enhances vegetation photosynthesis, because a higher blue/red light ratio within the diffuse radiation may lead to higher light use efficiency (Gu et al., 2002; Alton et al., 2007). For example, the sharply increased diffuse radiation induced by the 1991 Mount Pinatubo eruption enhanced the noontime vegetation productivity of a deciduous forest in the next 2 years (Gu et al. 2003). Besides volcanic aerosols, clouds could also reduce the total and direct radiation, while increase the proportion of diffuse radiation. Yuan et al. (2010) found that the higher LUE at European forests than North America was because of the higher ratio of cloudy days in Europe. Yuan et al. (2014) further proved that the significantly underestimated GPP during cloudy days by six LUE models was because the effects of diffuse radiation on LUE were neglected in these models.

Thirdly, atmospheric vapor pressure deficit (VPD) is another factor that should be included in GPP models. As an important driver of atmospheric water demand for plants, VPD influences terrestrial ecosystem function and photosynthesis (Rawson et al., 1977; Yuan, et al., 2019). Rising air temperature increases the saturated vapor pressure at a rate of ~7%/K according to the Classius–Clapeyron relationship, and therefore, VPD will increase if the atmospheric water vapor content does not increase by exactly the same amount as the saturated vapor pressure. Numerous studies indicated significant changes in the relative humidity (ratio of actual water vapor pressure to saturated water vapor pressure) in both humid areas and continental areas located far from oceanic humidity (Van Wijngaarden and Vincent, 2004; Pierce et al., 2013). In particular, the global averaged land surface relative humidity decreased sharply after the late 1990s (Simmons et al. 2010; Willett et al. 2014). The leaf and canopy photosynthetic rate declines when the atmospheric VPD increases due to stomatal closure (Fletcher et al., 2007). A recent study highlighted that increases in VPD rather than changes in precipitation would be a dominant influence on vegetation productivity (Konings et al., 2017). However, currently the influence of long-term VPD variations is not well expressed in many LUE models.

We have developed a LUE model, namely the EC-LUE model, by integrating remote sensing data and eddy covariance data to simulate daily GPP (Yuan et al., 2007; 2010). The model has been evaluated using the observations at EC towers located in Europe, North America, China, and East Asia, covering various ecosystem types (Yuan et al., 2007; 2010; Li et al., 2013). In this study, we revised the EC-LUE model by integrating the impacts of several environmental variables (i.e., atmospheric

CO_2 concentration, radiation components, and atmospheric VPD) across a long-term temporal scale. Firstly, we evaluated the effectiveness of the revised EC-LUE model in determining the spatial, seasonal, and interannual variations in GPP from multiple eddy covariance sites. Secondly, a global GPP dataset at 0.05 ° spatial resolution was generated based on the optimized model. Finally, we analyzed the contributions of the aforementioned environmental variables to the global GPP and discussed the spatial and interannual variations in GPP from different datasets.

2 Data and Methods

2.1 Data from the eddy covariance towers

The FLUXNET2015 dataset (http://www.fluxdata.org) includes over 200 variables of carbon fluxes, energy fluxes, and meteorological variables collected and processed at sites by the FLUXNET community. In our study, ninety-five EC sites in FLUXNET2015 dataset were utilized to optimize the parameters and evaluate the performance of the revised EC-LUE model, including nine major terrestrial ecosystem vegetation types (Table 1): evergreen broadleaf forests (EBF), evergreen needleleaf forests (ENF), deciduous broadleaf forests (DBF), mixed forests (MF), grasslands (GRA), savannas (SAV), shrubland (SHR), wetlands (WET), and croplands (CRO). More information about the characteristics of these sites can be referred to the FLUXNET website. For each site, the daily GPP, PAR, air temperature (Ta), and VPD were used in our study. The GPP variable (GPP_NT_VUT_REF) used in this study was estimated from night-time partitioning method. The corresponding net ecosystem exchange (NEE) was generated using variable friction velocity (USTAR) threshold for each year (VUT), in which 40 versions of NEE were created by using different percentiles of USTAR thresholds. The model efficiency between each version and the others 39 versions were calculated to test their similarities and the reference (REF) NEE was selected as the one with higher model efficiency sum (the most similar to the others 39). The daily meteorological variables were gap-filled or downscaled from the ERA-interim reanalysis dataset in both space and time (Vuichard and Papale, 2015). The gap-filled technique of the carbon flux measurements and meteorological variables is the marginal distribution sampling (MDS) method described in Reichstein et al. (2005). For each variable, we aggregated the daily values to 8-day time step. Only the 8-day measurements with more than 5-day valid values were used.

<<Table 1>>

2.2 Data at the global scale

The global scale datasets used in this study are shown in Table 2. The meteorological reanalysis dataset was derived from the second Modern-Era Retrospective analysis for Research and Applications (MERRA-2) dataset. It was produced by NASA's Global Modeling and Assimilation Office that used an upgraded version of the GEOS-5 (Rienecker et al., 2011). It has been validated carefully using surface meteorological datasets and enhanced assimilation system to reduce the uncertainty in various meteorological variables globally. In our study, we obtained the daily mean air temperature (T_a, ℃), mean dew point

temperature (T_d, ℃), total direct PAR (PAR_{dr}, MJ m^{-2} d^{-1}), and total diffuse PAR (PAR_{df}, MJ m^{-2} d^{-1}) at 0.625 °in longitude by 0.5 °in latitude from 1982 to 2017. VPD was calculated from air temperature and dew point temperature:

$$SVP = 6.112 \times e^{\frac{17.67T_a}{T_a+243.5}} \quad (1)$$

$$RH = e^{\frac{17.625T_d}{T_d+243.04}-\frac{17.625T_a}{T_a+243.04}} \quad (2)$$

$$VPD = SVP \times (1 - RH) \quad (3)$$

where SVP is the saturated vapor pressure (k Pa), and RH is the relative humidity. We aggregated the daily variables (air temperature, VPD, direct PAR, and diffuse PAR) to 8-day interval temporal resolution. And these variables were resampled to the spatial resolution of 0.05 °latitude by 0.05 °longitude using the bilinear interpolation method.

The 8-day Global LAnd Surface Satellite-leaf area index (GLASS LAI) dataset at 0.05 ° latitude by 0.05 ° longitude was adopted to indicate vegetation growth from 1982 to 2017. It was produced using the general regression neural networks (GRNNs) trained with the fused MOD15 LAI and CYCLOPES LAI and the preprocessed MODIS/AVHRR reflectance data over the BELMANIP sites (Xiao et al., 2016). Products validation and comparison showed that the GLASS LAI product was spatially complete and temporally continuous with lower uncertainty (Xu et al., 2018).

Additionally, the MCD12Q1 product with IGBP classification scheme was used as land cover map. The ISLSCP II C4 Vegetation Percentage map was used to separate the C3 and C4 crops. The NOAA's Earth System Research Laboratory (ESRL) CO_2 concentration dataset was used to express the CO_2 fertilization effect.

<<Table 2>>

2.3 The revised EC-LUE model

The terrestrial vegetation GPP can be expressed as follows in the revised EC-LUE model:

$$GPP = (\varepsilon_{msu} \times APAR_{su} + \varepsilon_{msh} \times APAR_{sh}) \times C_s \times \min(T_s, W_s) \quad (4)$$

where ε_{msu} is the maximum LUE of sunlit leaves; $APAR_{su}$ is the PAR absorbed by sunlit leaves; ε_{msh} is the maximum LUE of shaded leaves; $APAR_{sh}$ is the PAR absorbed by shaded leaves; C_s, T_s, and W_s represent the downward regulation scalars of atmospheric CO_2 concentration ($[CO_2]$), air temperature, and VPD on LUE ranging from 0 to 1; *min* represents the minimum value.

The effect of atmospheric CO_2 concentration on GPP is determined by the following equations (Farquhar et al., 1980; Collatz et al., 1991):

$$C_s = \frac{C_i - \varphi}{C_i + 2\varphi} \quad (5)$$

$$C_i = C_a \times \chi \quad (6)$$

where φ is the CO_2 compensation point in the absence of dark respiration (ppm); C_i is the leaf internal CO_2 concentration; C_a is the atmospheric CO_2 concentration; χ is the ratio of leaf internal to atmospheric CO_2 concentration which can be estimated as follows (Prentice et al., 2014; Keenan et al., 2016):

$$\chi = \frac{\varepsilon}{\varepsilon + \sqrt{\mathrm{VPD}}} \quad (7)$$

$$\varepsilon = \sqrt{\frac{356.51\mathrm{K}}{1.6\eta^*}} \quad (8)$$

where ε is a parameter related to the 'carbon cost of water', which means the sensitivity of VPD to χ; K is the Michaelis–Menten coefficient of Rubisco; η^* is the viscosity of water relative to its value at 25 ℃ (Korson et al., 1969).

$$\mathrm{K} = \mathrm{K_c}\left(1 + \frac{\mathrm{P_0}}{\mathrm{K_0}}\right) \quad (9)$$

where P_o is the partial pressure of O_2; K_c and K_o are the Michaelis–Menten constants for CO_2 and O_2 (Keenan et al., 2016):

$$\mathrm{K_c} = 39.97 \times \mathrm{e}^{\frac{79.43\times(\mathrm{T_a}-298.15)}{298.15\times\mathrm{R}\times\mathrm{T_a}}} \quad (10)$$

$$\mathrm{K_o} = 27480 \times \mathrm{e}^{\frac{36.38\times(\mathrm{T_a}-298.15)}{298.15\times\mathrm{R}\times\mathrm{T_a}}} \quad (11)$$

where T_a is air temperature (unit: K); R is the molar gas constant (8.314 J mol^{-1} K^{-1}).

T_s and W_s can be expressed as follows:

$$\mathrm{T_s} = \frac{(\mathrm{T_a}-\mathrm{T_{min}})\times(\mathrm{T_a}-\mathrm{T_{max}})}{(\mathrm{T_a}-\mathrm{T_{min}})\times(\mathrm{T_a}-\mathrm{T_{max}})-(\mathrm{T_a}-\mathrm{T_{opt}})\times(\mathrm{T_a}-\mathrm{T_{opt}})} \quad (12)$$

$$\mathrm{W_s} = \frac{\mathrm{VPD_0}}{\mathrm{VPD_0}+\mathrm{VPD}} \quad (13)$$

where T_{min}, T_{opt}, and T_{max} are the minimum, optimum, and maximum temperatures for vegetation photosynthesis, respectively (Yuan et al., 2007); VPD_0 is the half-saturation coefficient of the VPD constraint equation (k Pa).

$APAR_{su}$ and $APAR_{sh}$ can be expressed as follows (Chen et al., 1999):

$$\mathrm{APAR_{su}} = \left(\mathrm{PAR_{dir}} \times \frac{\cos(\beta)}{\cos(\theta)} + \frac{\mathrm{PAR_{dif}}-\mathrm{PAR_{dif,u}}}{\mathrm{LAI}} + \mathrm{C}\right) \times \mathrm{LAI_{su}} \quad (14)$$

$$\mathrm{APAR_{sh}} = \left(\frac{\mathrm{PAR_{dif}}-\mathrm{PAR_{dif,u}}}{\mathrm{LAI}} + \mathrm{C}\right) \times \mathrm{LAI_{sh}} \quad (15)$$

$$\mathrm{PAR_{dif,u}} = \mathrm{PAR_{dif}} \times \exp\left(\frac{-0.5\times\Omega\times\mathrm{LAI}}{\cos(\bar{\theta})}\right) \quad (16)$$

where PAR_{dir} is the direct PAR; PAR_{dif} is the diffuse PAR; $PAR_{dif,u}$ is the diffuse PAR under the canopy; C represents the multiple scattering effects of direct radiation; Ω is the clumping index, which is set according to vegetation types (Tang et al., 2007); θ is the solar zenith angle; β is the mean leaf–sun angle, which is set to 60 °; $\bar{\theta}$ is the representative zenith angle for diffuse radiation transmission and can be expressed by LAI (Chen et al., 1999):

$$\cos(\bar{\theta}) = 0.537 + 0.025 \times \mathrm{LAI} \quad (17)$$

The LAIs of shaded leaves (LAI_{sh}) and sunlit leaves (LAI_{su}) in Eqs. (14) and (15) are computed following Chen et al (1999):

$$\mathrm{LAI_{su}} = 2 \times \cos(\theta) \times \left(1 - \mathrm{e}^{-0.5\times\Omega\times\frac{\mathrm{LAI}}{\cos(\theta)}}\right) \quad (18)$$

$$\mathrm{LAI_{sh}} = \mathrm{LAI} - \mathrm{LAI_{su}} \quad (19)$$

2.4 Model calibration and validation

Cross-validation method was used to calibrate and validate the revised EC-LUE model. Fifty percent of the sites were randomly selected to calibrate model parameters for each vegetation type, and the remaining 50% of the sites were used to validate the model. This parameterization process was repeated until all possible combinations of 50% sites were achieved for each vegetation type. The nonlinear regression procedure (Proc NLIN) in the Statistical Analysis System (SAS, SAS Institute Inc., Cary, NC, USA) was applied to optimize the model parameters (ε_{msu}, ε_{msh}, φ, and VPD_0) using 8-day estimated GPP based on EC measurements. The mean GPP simulations of 8-day from all validation runs only were used to model validation. Mean calibrated parameter values from all model runs were used to simulate GPP over the global scale (Table 3). Three metrics, the coefficient of determination (R^2), RMSE, and bias (the difference between observations and simulations) were adopted to evaluate the performance of the revised EC-LUE model. Additionally, Kendall's coefficient of rank correlation τ (Kanji, 1999) was used to quantify the agreement of seasonal changes between the simulated and tower estimated GPP. The Kendall coefficient measured the tendency coherence between predicted and observed GPP by comparing the ranks assigned to successive pairs. If $\mathrm{GPP_{sim,j}} - \mathrm{GPP_{sim,i}}$ and $\mathrm{GPP_{obs,j}} - \mathrm{GPP_{obs,i}}$ have the same sign (positive or negative), the pair would be concordant, or discordant. A time-series data with n observations, the Kendall's coefficient of rank correlation τ can be expressed:

$$\tau = \frac{\mathrm{C-D}}{\mathrm{n(n-1)/2}} \quad (20)$$

where $\mathrm{n(n-1)/2}$ is the total combination of pairs, C is the number of concordant pairs, and D is the number of discordant pairs. The Kendall's coefficient ranged from -1 ($\mathrm{C} = 0$) to 1 ($\mathrm{D} = 0$). The Kendall's coefficient is much closer to 1, which means a stronger positive relationship between the seasonal patterns of the simulated and tower estimated GPP.

Using the averaged value of the optimized parameters (Table 3), a global GPP dataset at $0.05° \times 0.05°$ spatial resolution and 8-day temporal resolution over 1982-2017 was produced.

<<Table 3>>

2.5 Environmental contributions to long-term changes in GPP

To evaluate the contribution of the major environmental variables to GPP, including the atmospheric CO_2 concentration ($[CO_2]$), climate, and satellite-based LAI, two types of experimental simulations were performed. The first simulation experiment (S_{ALL}) was a normal model run, with all the environmental drivers changing over time. In the second type of simulation experiments (S_{CLI0}, S_{LAI0}, and S_{CO20}), two driving factors could be varied with time while maintaining the third constant at an initial baseline level. For example, the S_{CLI0} simulation experiment allowed the LAI and atmospheric $[CO_2]$ to vary with time while the climate variables were kept constant at 1982 values. The S_{LAI0} (S_{CO20}) simulation experiments kept LAI (atmospheric $[CO_2]$) constant at 1982 values and varied the other two variables.

Considering the differences between the simulation results of the first type (S_{ALL}) and the second type (S_{CO20} and S_{LAI0}) of experiments, the GPP sensitivities to atmospheric $[CO_2]$ (β_{CO2}) and LAI (β_{LAI}) were estimated as follows:

$$\Delta GPP_{(S_{ALL}-S_{CO2_0})i} = \beta_{CO2} \times \Delta CO2_{(S_{ALL}-S_{CO2_0})i} + \varepsilon \quad (21)$$

$$\Delta GPP_{(S_{ALL}-S_{LAI_0})i} = \beta_{LAI} \times \Delta LAI_{(S_{ALL}-S_{LAI_0})i} + \varepsilon \quad (22)$$

where ΔGPP_i, $\Delta CO2_i$, and ΔLAI_i denote the differences in the GPP simulations, atmospheric [CO_2], and *LAI* between the two model experiments from 1982 to 2017, and ε is the stochastic error term.

The GPP sensitivities to the three climate variables: air temperature (β_{Ta}), VPD (β_{VPD}), and PAR (β_{PAR}) were calculated using a multiple regression approach:

$$\Delta GPP_{(S_{ALL}-S_{CLI_0})i} = \beta_{Ta} \times \Delta Ta_{(S_{ALL}-S_{CLI_0})i} + \beta_{VPD} \times \Delta VPD_{(S_{ALL}-S_{CLI_0})i} + \beta_{PAR} \times \Delta PAR_{(S_{ALL}-S_{CLI_0})i} + \varepsilon \quad (23)$$

where ΔTa_i, ΔVPD_i, and ΔPAR_i denote the differences in Ta, VPD, and PAR time series between the two model experiments (S_{ALL} and S_{CLI0}), respectively. The regression coefficient β was estimated using the maximum likelihood analysis.

3 Results

3.1 Model performance

In general, the revised EC-LUE model could effectively reproduce the spatial, seasonal, and annual variations in the tower estimated GPP at most sites (Figs. 1–3). The revised EC-LUE model explained 71% and 64% of the spatial variations in GPP across all the EC sites by using the tower-derived meteorology data and the meteorological reanalysis dataset, respectively (Fig. 1).

<<Figure 1>>

Similarly, the revised EC-LUE model also shows a good performance in reproducing the seasonal variations in the GPP at most EC sites (Fig. 2). In Fig. 2, we compared the modeled GPP and tower GPP at 8-day step for each site to examine the capacity of our model in reproducing the seasonal variations. The averaged R^2 were 0.81 and 0.76 by using the tower-derived meteorology data and the meteorological reanalysis dataset, respectively. Using the tower-derived meteorology data, over 95% of the sites showed high R^2 (>0.5). The low R^2 (< 0.4) sites (i.e., MY-PSO, BR-Sa1 and BR-Sa3) were tropical forests without pronounced seasonal patterns of GPP (Fig. 2a). The RMSE and the absolute value of bias varied from 0.69 (CN-Du2) to 5.63 (US-Ne2) g C m^{-2} d^{-1} and from 0.004 (CA-NS1) to 2.40 (CA-TP2) g C m^{-2} d^{-1}, respectively. The averaged RMSE and the absolute value of bias over all the sites were 2.13 and 0.81 g C m^{-2} d^{-1}, respectively (Fig. 2b–c). The averaged Kendall's correlation coefficient (τ) was 0.63, indicating that the model simulated GPP had a strong seasonal coherence with tower estimated GPP. Similar to R^2, the lower Kendall's correlation coefficient (τ) value sites were also located in the tropical forest areas. Additionally, there was no obvious difference between the seasonal GPP performance by using the tower-derived meteorology data and the meteorological reanalysis dataset (Fig. 2).

<< Figure 2>>

The ability of the LUE models to reproduce the interannual variations in GPP was investigated at 55 EC towers with observations greater than 5-years (Table 1; Fig. 3). We examined the relations between the mean annual GPP simulations

and observations at each site and used the coefficient correlation (R^2) and slope of the regression relationship to investigate the model capability in simulating the interannual variations in GPP. The result showed that the revised EC-LUE model could effectively determine the interannual variations in GPP (Fig. 3). Approximately 42% and 40% of the sites showed higher R^2 values (>0.5) by using the tower-derived meteorology data and the meteorological reanalysis dataset (Fig. 3a). The averaged R^2 for the revised EC-LUE model was 0.44 by using the tower-derived meteorology data, which was significantly higher than the original EC-LUE model (R^2 = 0.36) and other LUE models (R^2 ranged from 0.06 to 0.30 with an average value of 0.16) (Fig. 3c). The averaged R^2 for the revised EC-LUE model was 0.42 by using the meteorological reanalysis dataset. The averaged slopes of the revised EC-LUE model were 0.60 and 0.57 by using the tower-derived meteorology data and the meteorological reanalysis dataset (Fig. 3c).

<<Figure 3>>

3.2 Spatio-temporal patterns of global GPP

A global GPP dataset at 0.05 °latitude by 0.05 °longitude and 8-day interval was generated ranging from 1982 to 2017 based on the revised EC-LUE model. The long-term averaged value of the global summed GPP was 106.2 ± 2.9 Pg C yr^{-1} across the vegetated area. Fig. 4 shows the global distribution pattern of the annual averaged GPP for each pixel. The GPP was high over the tropical forest areas, such as Amazon and Southeast Asia, where the moisture and temperature conditions are sufficient for photosynthesis (Fig. 4a). The GPP decreased with the decreasing gradients of temperature and precipitation (Fig. 4b). The moderate GPP was located in temperate and subhumid regions; and the lowest GPP was located in arid or cold regions, where either precipitation or temperature is limited (Fig. 4b).

<<Figure 4>>

GPP trends over the period of 1982–2017 were determined for each pixel using a linear regression analysis (Fig. 5). In general, the revised EC-LUE model predicted an increased trend in the annual mean GPP from 1982 to 2017. Approximately 69.5% of the vegetated areas, mainly located in temperate and humid regions, showed increased trends. The spatial pattern of the GPP trend along with the temperature and precipitation gradients was more heterogeneous than that of the mean annual GPP (Fig. 4b; Fig. 5b). The decreased GPP was found in the tropic regions, especially in the Amazon forest. The extremely cold or arid areas exhibited less variations in GPP (Fig. 5b).

<<Figure 5>>

3.3 Contributions of environmental variables to GPP

To quantify the contributions of the environmental variables to the long-term changes in GPP, we explored the sensitivity of global summed GPP to climate variables (i.e., VPD, Ta, and PAR), LAI, and atmospheric CO_2 (Fig. 6). The global summed GPP generated from different experimental simulations (section 2.5) exhibited differently in terms of the annual mean value, trend, and standard deviation (Fig. 6a). The normal simulated GPP (S_{ALL} GPP, all the environmental drivers changing over time) significantly increased at the rate of 0.15 Pg C yr^{-1}, while the increasing rate of S_{CLI0} GPP (climate variables were kept

constant at 1982 values) was even greater (0.41 Pg C yr^{-1}). On the contrary, the S_{LAI0} GPP (LAI was kept constant at 1982 values) and the S_{CO20} GPP (atmospheric [CO_2] was kept constant at 1982 values) showed insignificantly decreasing trend at the rate of -0.04 Pg C yr^{-1} and -0.07 Pg C yr^{-1} (Fig. 6a). The GPP sensitivity analysis showed that the global GPP decreased by 6.67 ± 5.04 Pg C with a 0.1 kPa increase in VPD, which was comparable to the increase in GPP with 0.1 unit greening of LAI (i.e., β_{LAI} = 4.78 ± 0.72 Pg C 0.1 $unit^{-1}$) or 100 MJ increase in PAR (i.e., β_{PAR} = 5.73 ± 3.22 Pg C 100 MJ^{-1}) (Fig. 6b). The global GPP increased by 12.31 ± 0.61 Pg C with a 100 ppm^{-1} rise of atmospheric [CO_2] (i.e., β_{CO2} = 12.31 ± 0.61 Pg C 100 ppm^{-1}). Over the period of 1982–2017, the increased VPD resulted in the global GPP decreases of −0.17 ± 0.06 Pg C yr^{-1}, which could partly counteract the fertilization effect of CO_2 (0.22 ± 0.07 Pg C yr^{-1}). The global GPP showed a decreased trend after 2001 due to the joint effect of increased VPD and decreased PAR (Fig. 6c). While the increased trend of GPP before 2000 was affected by the rising atmospheric [CO_2], greening of LAI, and increased PAR (Fig. 6c).

<<Figure 6>>

4 Discussion

4.1 Model accuracy analysis

Numerous studies have shown that most GPP models can reproduce the spatial changes in GPP but failed to reproduce the temporal variations (Keenan et al., 2012; Yuan et al., 2014). Therefore, the capacity to reproduce realistic interannual variations for a GPP model is significantly important. In our study, the revised EC-LUE model performed a higher accuracy in reproducing the interannual variations in GPP than did the original EC-LUE model and other LUE models. Yuan et al. (2014) reported that the averaged slope of the regression relation between the mean annual GPP simulated by seven LUE models and the mean annual GPP estimated from EC tower ranged from 0.19 to 0.56 (Fig. 3c). While the revised EC-LUE model showed a higher slope of regression relation (0.60), which is much closer to 1 than that obtained from other LUE models (Fig. 3c). The VPM GPP showed less interannual variations across most biomes (R^2 <0.5), probably because of the insensitivity of the environmental stress factors at the interannual scale (Zhang et al., 2017). In contrast, 42% of the sites showed higher R^2 values (>0.5) for the revised EC-LUE model. The improvements of the revised EC-LUE model in reproducing interannual variations are owing to the integration of several important environmental drivers for vegetation production (i.e., atmospheric CO_2 concentration, radiation components, and VPD), which exhibited large variations and contributed significantly to vegetation production at interannual scale.

By integrating the atmospheric CO_2 concentration, the revised EC-LUE model suggested a CO_2 sensitivity (β_{CO2}) of 12.31 ± 0.61 Pg C per 100 ppm (Fig. 6b), which indicates an increase of 11.6% in GPP with a rise of 100 ppm in atmospheric [CO_2]. Our estimate is comparable to the observed response of NPP to the increased CO_2 in the FACE experiments (13% per 100 ppm) and estimates of other ecosystem models (5–20% per 100 ppm) (Piao et al., 2013). The elevated atmospheric CO_2 concentration substantially contributes to vegetation productivity.

The evaporation fraction (EF), namely the ratio of evapotranspiration (ET) to net radiation (Rn), was used to indicate the water stress on vegetation growth in the original EC-LUE model (Yuan et al., 2007; 2010). While the atmospheric VPD was used to indicate water stress to avoid the aggregated errors from ET simulations in the revised EC-LUE model. Physiologically, vegetation production is sensitive to both atmospheric VPD and soil moisture availability to roots. Recent studies highlighted that the increase in VPD had a larger limitation to the surface conductance and evapotranspiration than soil moisture over short time scales in many biomes (Novick et al., 2016; Sulman et al., 2016). Other studies have also suggested substantial impacts of VPD on vegetation growth (de Cárcer et al., 2018; Ding et al., 2018), forest mortality (Williams et al., 2013), and crop yields (Lobell et al., 2014). It is increasingly important to integrate the atmospheric water constraint to the carbon and water flux modeling.

4.2 Comparison of global GPP products

Global and regional GPP estimates remain highly uncertain despite the substantial advances in remote sensing technology, ground observations, and theory of carbon flux modeling (Zheng et al., 2018; Ryu et al., 2019). At regional scale, we compared the annual mean GPP between the revised EC-LUE model and other models across the bioclimatic zones in the Köppen-Geiger climate classification map (Beck et al., 2018) (Fig. 7). The GPP of the revised EC-LUE model was comparable to the mean value of other models for each bioclimatic zone (Fig. 7a). The GPP of different models exhibited large discrepancies in tropical regions (Af/Am/Aw) (Fig. 7a). The correlations (R^2) of GPP across all the bioclimatic zones between the revised EC-LUE model and other models ranged from 0.73 (LPX-Bern) to 0.95 (FLUXCOM MARS, FLUXCOM RF) (Fig. 7b).

<<Figure 7>>

At global scale, our study showed large differences in the magnitude of global GPP estimated by various models varying from 92.7 to 168.7 Pg C yr^{-1} (Figs. 8–9). The LUE models simulated the global GPP ranging from 92.7 to 133.7 Pg C yr^{-1} (Fig. 9a1). Several machine learning approaches estimated the global GPP ranging from 111.0 to 144.2 Pg C yr^{-1} (Fig. 9a2). A comparison of ten global terrestrial ecosystem models of TRENDY showed that the global GPP ranged from 107.8 to 154.9 Pg C yr^{-1} (Fig. 9a3). The revised EC-LUE model quantified the mean global GPP from 1982 to 2017 as 106.2 $\pm$ 2.9 Pg C yr^{-1}. Other studies also support the conclusion that there are large uncertainties in the GPP estimates. By comparing diverse GPP models and products, Anav et al. (2015) reported that the global GPP ranged from 112 to 169 Pg C yr^{-1}. Seven satellite-based LUE models estimated the global GPP ranged from 95.1 to 139.7 Pg C yr^{-1} over the period of 2000–2010 (Cai et al., 2014).

<<Figure 8>>

The interannual variability and trend in GPP also vary substantially with different models. This study showed that the interannual variability (standard deviation) ranged from 0.32 to 5.89 Pg C yr^{-1}, with the trends varying from −0.05 to 0.84 Pg C yr^{-1} (Fig. 9). The biophysical models showed large interannual variability, with the standard deviation ranging from 1.38 to 5.89 Pg C yr^{-1}. The LUE models estimated the interannual variability varied from 1.30 to 3.13 Pg C yr^{-1}. In contrast, the

machine learning models exhibited less interannual variability with standard deviation under 1.0 Pg C yr^{-1}. The interannual variability of the revised EC-LUE model was 2.9 Pg C yr^{-1} (Figs. 9b1–b3). In general, the GPP interannual variability before the year 2000 year was greater than that after the year 2001 for most of the biophysical models and LUE models (Figs. 9b1–b3). Most GPP models showed an increased trend or insignificant trend during all valid years and before 2000. Similar to the standard deviation, the trends of machine learning models were less than other models. Compared with the other models, CLASS and the revised EC-LUE model showed a significant decreasing trend after 2001 (Figs. 9c1–c3), probably because of the joint effect of increased VPD and decreased PAR (Fig. 6c).

<<Figure 9>>

4.3 Model uncertainty

The revised EC-LUE model showed the lowest accuracy for the evergreen broadleaf forests in the tropic areas (Fig. 2). Similarly, other satellite-based models exhibited a large uncertainty in the GPP simulations over tropical forest areas (Ryu et al., 2011; Yuan et al., 2014). MODIS GPP product (MOD17) underestimated the GPP at high productivity sites over the tropical evergreen forests (de Almeida et al., 2018). Regarding the quality of satellite data, a high cloud cover exists over tropical regions, introducing large uncertainties to FAPAR/LAI and other vegetation indices (e.g., NDVI and EVI). For example, less reliable MOD15 FAPAR data from January to April because of the cloudiness contamination, which could substantially affect the seasonality of GPP estimates (de Almeida et al., 2018). Furthermore, the quality of satellite data even affects the evaluation of the interannual variations. Saleska et al. (2007) reported that a large scale green-up in the Amazon evergreen forests during the drought in 2005 using MODIS EVI data. However, an opposite conclusion was arrived when cloud-contaminated data were excluded from the analysis, showing no obvious green-up in the Amazon evergreen forests during the drought in 2005 (Samanta et al., 2010). Additionally, several subsequent studies found increased LAI and EVI during the dry season in the Amazon evergreen forests; however, a recent study highlighted that the apparent seasonal changes in EVI result from the variations in the sun-sensor geometry rather than vegetation greenness (Morton et al., 2014). The latest study highlighted that the aggregate canopy phenology rather than the climate changes is the main cause of the seasonal changes in photosynthesis in evergreen broadleaf forests (Wu et al., 2016). In particular, the new leaf growing synchronously with dry season litterfall may shift the old canopy to be younger, which can explain the significant seasonal increase (~27%) in the ecosystem photosynthesis. Therefore, the vertical changes in leaf age and photosynthesis ability with canopy depth are important to simulate the seasonal variations in carbon flux in tropical forests (Wu et al., 2017). These leaf trait related parameters can be simulated from the narrow-band spectra of leaves (Serbin et al., 2012; Dechant et al., 2017). Nevertheless, because of the limitation in obtaining the large scale hyperspectral remote sensing data, regional or global estimation of these parameters are currently unavailable.

The revised EC-LUE model does not integrate the regulation of soil nitrogen content on vegetation production. Atmospheric nitrogen deposition has exhibited a large increasing trend in the past few decades because of the excessive fossil fuel combustion in the industrial and transportation sectors and the abuse of nitrogenous fertilizer in the agricultural practice

(Galloway et al., 2004). And the global land atmospheric nitrogen deposition is expected to further increase dramatically from 25–40 Tg N yr^{-1} in the 2000s to 60–100 Tg N yr^{-1} in 2100 (Lamarque et al., 2005). A meta-analysis of worldwide nitrogen addition experiments found that nitrogen addition could have a significantly positive effect on vegetation productivity (Liu and Greaver, 2009). As most terrestrial ecosystems are nitrogen limited, quantifying the spatio-temporal distributions of vegetation nitrogen content at large scales is essential to improve the accuracy of carbon flux estimation. Several studies quantified the leaf nitrogen content by detecting the nitrogen absorption spectra from the narrow-band of hyperspectral data (Cho, 2007). However, leaf water, starch, lignin, and cellulose overlap with the absorption characters of nitrogen in the shortwave infrared bands, making it difficult to retrieve the nitrogen content (Kokaly and Clark, 1999). What's more, canopy structures, background, and illumination/viewing geometry can further decrease the capacity to detect leaf nitrogen (Yoder and Pettigrew-Crosby, 1995; Knyazikhin et al., 2013). Advances in inversion and statistical models of leaf or canopy nitrogen have emerged (Asner et al., 2011; Dechant et al., 2017; Wang et al., 2018), but these methods require further evaluation over large regions and the global map of leaf or canopy nitrogen is not available yet.

Additionally, the uncertainty of the revised EC-LUE model may arise by scale mismatches between eddy covariance flux footprint and input dataset. The eddy covariance flux footprint is generally less than 3 km^2 and varies depending on the wind speed, wind direction and atmospheric stability (Tan et al., 2006). In our studies, the revised EC-LUE model was run at 0.05 degree (~5 km^2) spatial resolution. The uncertainty of simulated GPP introduced by the scale effect is inevitable but smaller than that introduced by the model structures, parameters or input datasets (Sjostrom et al., 2013; Zheng et al., 2018).

5 Data availability

The $0.05° \times 0.05°$ global GPP dataset for 1982-2017 is available at https://doi.org/10.6084/m9.figshare.8942336 (Zheng et al., 2019). The dataset is provided in hdf format at 8-day interval. The valid value is ranged from 0 to 3000, and the background filled value is 65535. The scale factor of the data is 0.01. Each hdf file represents an 8-day GPP at daily value (unit: g C m^{-2} day^{-1}). To obtain the summation of each 8-day (or 5-day or 6-day) period, please multiply the GPP value by corresponding days (8 for the first 45 values, and 5 or 6 for the last value in a year).

6 Conclusion

In this study, we produced a long-term global GPP dataset by integrating several major long-term environmental variables into a light use efficiency model, including atmospheric CO_2 concentration, radiation components, and atmospheric water vapor pressure. These environmental variables showed substantial long-term changes and contributed significantly to vegetation production at interannual scale. The revised EC-LUE performed well in simulating the spatial, seasonal, and interannual variations in GPP across the globe. Particularly, it has a unique superiority in reproducing the interannual variations in GPP (R^2 = 0.44) compared with the original EC-LUE model (R^2 = 0.36) and other LUE models (R^2 ranged

from 0.06 to 0.30 with an average value of 0.16). The GPP dataset derived from the revised EC-LUE model provides an alternative and reliable estimates of global GPP at the long-term scale by integrating the important environmental variables.

Author contributions. W. Yuan and Y. Zheng designed the research, performed the analysis, and wrote the paper; R. Shen, Y. Wang, and X. Li performed the analysis; S. Liu, S. Liang, J. Chen, W. Ju, and L. Zhang edited and revised the manuscript.

Competing interests. The authors declare that they have no conflict of interest.

Acknowledgements

This study was supported by National Key Basic Research Program of China (2016YFA0602701), Changjiang Young Scholars Programme of China (Q2016161), Training Project of Sun Yat-sen University (16lgjc53), Fok Ying Tung Education Foundation (151015), and Beijing Normal University Project (2015KJJCA14). The covariance data used in the study was acquired and shared by the FLUXNET community, including these networks: AmeriFlux, AfriFlux, AsiaFlux, CarboAfrica, CarboEuropeIP, CarboItaly, CarboMont, ChinaFlux, Fluxnet-Canada, GreenGrass, ICOS, KoFlux, LBA, NECC, OzFlux-TERN, TCOS-Siberia, and USCCC. The ERA-Interim reanalysis data are provided by ECMWF and processed by LSCE. The FLUXNET eddy covariance data processing and harmonization was carried out by the European Fluxes Database Cluster, AmeriFlux Management Project, and Fluxdata project of FLUXNET, with the support of CDIAC and ICOS Ecosystem Thematic Center, and the OzFlux, ChinaFlux and AsiaFlux offices.

References

Ainsworth, E.A., Long, S.P.: What have we learned from 15 years of free-air CO_2 enrichment (FACE)? A meta-analytic review of the responses of photosynthesis, canopy, New Phytol., 165, 351-371, doi:10.1111/j.1469-8137.2004.01224.x, 2005.

Alton, P.B., North, P.R., Los, S.O.: The impact of diffuse sunlight on canopy light-use efficiency, gross photosynthetic product and net ecosystem exchange in three forest biomes, Global Change Biol., 13, 776-787, doi:10.1111/j.1365-2486.2007.01316.x, 2007.

Anav, A., Friedlingstein, P., Beer, C., Ciais, P., Harper, A., Jones, C., Murray-Tortarolo, G., Papale, D., Parazoo, N.C., Peylin, P., Piao, S., Sitch, S., Viovy, N., Wiltshire, A., Zhao, M.: Spatiotemporal patterns of terrestrial gross primary production: A review, Rev. Geophys., 53, 785-818, doi:10.1002/2015rg000483, 2015.

Asner, G.P., Martin, R.E., Knapp, D.E., Tupayachi, R., Anderson, C., Carranza, L., Martinez, P., Houcheime, M., Sinca, F., Weiss, P.: Spectroscopy of canopy chemicals in humid tropical forests, Remote Sens. Environ., 115, 3587-3598, doi:10.1016/j.rse.2011.08.020, 2011.

Beck, H.E., Zimmermann, N.E., McVicar, T.R., Vergopolan, N., Berg, A., Wood, E.F.: Present and future Koppen-Geiger climate classification maps at 1-km resolution, Scientific Data, doi:510.1038/sdata.2018.214, 2018.

Cai, W., Yuan, W., Liang, S., Zhang, X., Dong, W., Xia, J., Fu, Y., Chen, Y., Liu, D., Zhang, Q.: Improved estimations of gross primary production using satellite-derived photosynthetically active radiation, J. Geophys. Res. G: Biogeosci., 119, 110-123, doi:10.1002/2013jg002456, 2014.

Cai, W., Yuan, W., Liang, S., Liu, S., Dong, W., Chen, Y., Liu, D., Zhang, H.: Large Differences in Terrestrial Vegetation Production Derived from Satellite-Based Light Use Efficiency Models, Remote Sens., 6, 8945-8965, doi:10.3390/rs6098945, 2014.

Canadell, J.G., Le Quere, C., Raupach, M.R., Field, C.B., Buitenhuis, E.T., Ciais, P., Conway, T.J., Gillett, N.P., Houghton, R.A., Marland, G.: Contributions to accelerating atmospheric CO_2 growth from economic activity, carbon intensity, and efficiency of natural sinks, Proc. Natl. Acad. Sci. U.S.A., 104, 18866-18870, doi:10.1073/pnas.0702737104, 2007.

Chen, J.M., Liu, J., Cihlar, J., Goulden, M.L.: Daily canopy photosynthesis model through temporal and spatial scaling for remote sensing applications, Ecol. Modell., 124, 99-119, doi:10.1016/s0304-3800(99)00156-8, 1999.

Cho, M.A., Skidmore, A., Corsi, F., van Wieren, S.E., Sobhan, I.: Estimation of green grass/herb biomass from airborne hyperspectral imagery using spectral indices and partial least squares regression, International Journal of Applied Earth Observation and Geoinformation, 9, 414-424, doi:10.1016/j.jag.2007.02.001, 2007.

Collatz, G.J., Ball, J.T., Grivet, C., Berry, J.A.: Physiological and environmental regulation of stomatal conductance, photosynthesis and transpiration: a model that includes a laminar boundary layer, Agric. For. Meteorol., 54, 107-136, 1991.

de Almeida, C.T., Delgado, R.C., Galvao, L.S., de Oliveira Cruz e Aragao, L.E., Concepcion Ramos, M.: Improvements of the MODIS Gross Primary Productivity model based on a comprehensive uncertainty assessment over the Brazilian Amazonia, ISPRS J. Photogramm. Remote Sens., 145, 268-283, doi:10.1016/j.isprsjprs.2018.07.016, 2018.

de Cárcer, P.S., Vitasse, Y., Peñuelas, J., Jassey, V.E.J., Buttler, A., Signarbieux, C.: Vapor-pressure deficit and extreme climatic variables limit tree growth, Global Change Biol., 24, 1108-1122, doi:10.1111/gcb.13973, 2018.

Dechant, B., Cuntz, M., Vohland, M., Schulz, E., Doktor, D.: Estimation of photosynthesis traits from leaf reflectance spectra: Correlation to nitrogen content as the dominant mechanism, Remote Sens. Environ., 196, 279-292, doi:10.1016/j.rse.2017.05.019, 2017.

Ding, J., Yang, T., Zhao, Y., Liu, D., Wang, X., Yao, Y., Peng, S., Wang, T., Piao, S.: Increasingly Important Role of Atmospheric Aridity on Tibetan Alpine Grasslands, Geophys. Res. Lett., 45, 2852-2859, doi:10.1002/2017gl076803, 2018.

Farquhar, G.D., von Caemmerer, S., Berry, J.A.: A biochemical model of photosynthetic CO_2 assimilation in leaves of C 3 species, Planta, 149, 78-90, doi:10.1007/bf00386231, 1980.

Fletcher, A.L., Sinclair, T.R., Allen, L.H.: Transpiration responses to vapor pressure deficit in well watered 'slow-wilting' and commercial soybean, Environ. Exp. Bot., 61, 145-151, doi:10.1016/j.envexpbot.2007.05.004, 2007.

Galloway, J.N., Dentener, F.J., Capone, D.G., Boyer, E.W., Howarth, R.W., Seitzinger, S.P., Asner, G.P., Cleveland, C.C., Green, P.A., Holland, E.A., Karl, D.M., Michaels, A.F., Porter, J.H., Townsend, A.R., Vorosmarty, C.J.: Nitrogen cycles: past, present, and future, Biogeochemistry, 70, 153-226, doi:10.1007/s10533-004-0370-0, 2004.

Gilgen, H., Wild, M., Ohmura, A.: Means and trends of shortwave irradiance at the surface estimated from Global Energy Balance Archive data, J. Clim., 11, 2042-2061, doi:10.1175/1520-0442-11.8.2042, 1998.

Gu, L.H., Baldocchi, D., Verma, S.B., Black, T.A., Vesala, T., Falge, E.M., Dowty, P.R.: Advantages of diffuse radiation for terrestrial ecosystem productivity, J. Geophys. Res. D: Atmos., 10710.1029/2001jd001242, 2002.

Kanniah, K.D., Beringer, J., North, P., Hutley, L.: Control of atmospheric particles on diffuse radiation and terrestrial plant productivity: A review, Progress in Physical Geography-Earth and Environment, 36, 209-237, doi:10.1177/0309133311434244, 2012.

Ju, W., Chen, J.M., Black, T.A., Barr, A.G., Liu, J., Chen, B.: Modelling multi-year coupled carbon and water fluxes in a boreal aspen forest, Agric. For. Meteorol., 140, 136-151, doi:10.1016/j.agrformet.2006.08.008, 2006.

Jung, M., Reichstein, M., Schwalm, C.R., Huntingford, C., Sitch, S., Ahlstrom, A., Arneth, A., Camps-Valls, G., Ciais, P., Friedlingstein, P., Gans, F., Ichii, K., Ain, A.K.J., Kato, E., Papale, D., Poulter, B., Raduly, B., Rodenbeck, C., Tramontana, G., Viovy, N., Wang, Y.-P., Weber, U., Zaehle, S., Zeng, N.: Compensatory water effects link yearly global land CO2 sink changes to temperature, Nature, 541, 516-520, doi:10.1038/nature20780, 2017.

Kanji, G.K., 1999. 100 Statistical Tests. SAGE Publications, London.

Keenan, T.F., Baker, I., Barr, A., Ciais, P., Davis, K., Dietze, M., Dragon, D., Gough, C.M., Grant, R., Hollinger, D., Hufkens, K., Poulter, B., McCaughey, H., Raczka, B., Ryu, Y., Schaefer, K., Tian, H., Verbeeck, H., Zhao, M., Richardson, A.D.: Terrestrial biosphere model performance for inter-annual variability of land-atmosphere CO_2 exchange, Global Change Biol., 18, 1971-1987, doi:10.1111/j.1365-2486.2012.02678.x, 2012.

Keenan, T.F., Prentice, I.C., Canadell, J.G., Williams, C.A., Wang, H., Raupach, M., Collatz, G.J.: Recent pause in the growth rate of atmospheric CO_2 due to enhanced terrestrial carbon uptake, Nat. Commun., 710.1038/ncomms13428, 2016.

Knyazikhin, Y., Schull, M.A., Stenberg, P., Mottus, M., Rautiainen, M., Yang, Y., Marshak, A., Latorre Carmona, P., Kaufmann, R.K., Lewis, P., Disney, M.I., Vanderbilt, V., Davis, A.B., Baret, F., Jacquemoud, S., Lyapustin, A., Myneni, R.B.: Hyperspectral remote sensing of foliar nitrogen content, Proc. Natl. Acad. Sci. U.S.A., 110, E185-E192, doi:10.1073/pnas.1210196109, 2013.

Kokaly, R.F., Clark, R.N.: Spectroscopic determination of leaf biochemistry using band-depth analysis of absorption features and stepwise multiple linear regression, Remote Sens. Environ., 67, 267-287, doi:10.1016/s0034-4257(98)00084-4, 1999.

Konings, A.G., Williams, A.P., Gentine, P.: Sensitivity of grassland productivity to aridity controlled by stomatal and xylem regulation, Nat. Geosci., 10, 284-+, doi:10.1038/ngeo2903, 2017.

Korson, L., Drost-Hansen, W., Millero, F.J.: Viscosity of water at various temperatures, J. Phys. Chem., 73, 34-39, doi:10.1021/j100721a006, 1969.

Krupkova, L., Markova, I., Havrankova, K., Pokorny, R., Urban, O., Sigut, L., Pavelka, M., Cienciala, E., Marek, M.V.: Comparison of different approaches of radiation use efficiency of biomass formation estimation in Mountain Norway spruce, Trees-Structure and Function, 31, 325-337, doi:10.1007/s00468-016-1486-2, 2017.

Lamarque, J.F., Kiehl, J.T., Brasseur, G.P., Butler, T., Cameron-Smith, P., Collins, W.D., Collins, W.J., Granier, C., Hauglustaine, D., Hess, P.G., Holland, E.A., Horowitz, L., Lawrence, M.G., McKenna, D., Merilees, P., Prather, M.J., Rasch, P.J., Rotman, D., Shindell, D., Thornton, P.: Assessing future nitrogen deposition and carbon cycle feedback using a multimodel approach: Analysis of nitrogen deposition, J. Geophys. Res. D: Atmos., 11010.1029/2005jd005825, 2005.

Li, X.L., Liang, S.L., Yu, G.R., Yuan, W.P., Cheng, X., Xia, J.Z., Zhao, T.B., Feng, J.M., Ma, Z.G., Ma, M.G., Liu, S.M., Chen, J.Q., Shao, C.L., Li, S.G., Zhang, X.D., Zhang, Z.Q., Chen, S.P., Ohta, T., Varlagin, A., Miyata, A., Takagi, K., Saiqusa, N., Kato, T.: Estimation of gross primary production over the terrestrial ecosystems in China, Ecol. Modell., 261, 80-92, doi:10.1016/j.ecolmodel.2013.03.024, 2013.

Liu, L., Greaver, T.L.: A review of nitrogen enrichment effects on three biogenic GHGs: the CO_2 sink may be largely offset by stimulated N2O and CH4 emission, Ecol. Lett., 12, 1103-1117, doi:10.1111/j.1461-0248.2009.01351.x, 2009.

Liu, S., Bond-Lamberty, B., Boysen, L.R., Ford, J.D., Fox, A., Gallo, K., Hatfield, J., Henebry, G.M., Huntington, T.G., Liu, Z., Loveland, T.R., Norby, R.J., Sohl, T., Steiner, A.L., Yuan, W., Zhang, Z., Zhao, S.: Grand Challenges in Understanding the Interplay of Climate and Land Changes, Earth Interactions, 21, 1-43, doi:10.1175/ei-d-16-0012.1, 2017.

Liu, Y., Xiao, J., Ju, W., Zhu, G., Wu, X., Fan, W., Li, D., Zhou, Y.: Satellite-derived LAI products exhibit large discrepancies and can lead to substantial uncertainty in simulated carbon and water fluxes, Remote Sens. Environ., 206, 174-188, doi:10.1016/j.rse.2017.12.024, 2018.

Lobell, D.B., Roberts, M.J., Schlenker, W., Braun, N., Little, B.B., Rejesus, R.M., Hammer, G.L.: Greater Sensitivity to Drought Accompanies Maize Yield Increase in the US Midwest, Science, 344, 516-519, doi:10.1126/science.1251423, 2014.

Monteith, J.: Solar radiation and productivity in tropical ecosystems, J. Appl. Ecol., 9, 747-766, 1972.

Morton, D.C., Nagol, J., Carabajal, C.C., Rosette, J., Palace, M., Cook, B.D., Vermote, E.F., Harding, D.J., North, P.R.J.: Amazon forests maintain consistent canopy structure and greenness during the dry season, Nature, 506, 221-+, doi:10.1038/nature13006, 2014.

Norby, R.J., DeLucia, E.H., Gielen, B., Calfapietra, C., Giardina, C.P., King, J.S., Ledford, J., McCarthy, H.R., Moore, D.J.P., Ceulemans, R., De Angelis, P., Finzi, A.C., Karnosky, D.F., Kubiske, M.E., Lukac, M., Pregitzer, K.S., Scarascia-Mugnozza, G.E., Schlesinger, W.H., Oren, R.: Forest response to elevated CO_2 is conserved across a broad range of productivity, Proc. Natl. Acad. Sci. U.S.A., 102, 18052-18056, doi:10.1073/pnas.0509478102, 2005.

Norby, R.J., Wullschleger, S.D., Gunderson, C.A., Johnson, D.W., Ceulemans, R.: Tree responses to rising CO_2 in field experiments: implications for the future forest, Plant Cell Environ., 22, 683-714, doi:10.1046/j.1365-3040.1999.00391.x, 1999.

Novick, K.A., Ficklin, D.L., Stoy, P.C., Williams, C.A., Bohrer, G., Oishi, A.C., Papuga, S.A., Blanken, P.D., Noormets, A., Sulman, B.N., Scott, R.L., Wang, L., Phillips, R.P.: The increasing importance of atmospheric demand for ecosystem water and carbon fluxes, Nat. Clim. Change, 6, 1023-1027, doi:10.1038/nclimate3114, 2016.

Piao, S., Sitch, S., Ciais, P., Friedlingstein, P., Peylin, P., Wang, X., Ahlstrom, A., Anav, A., Canadell, J.G., Cong, N., Huntingford, C., Jung, M., Levis, S., Levy, P.E., Li, J., Lin, X., Lomas, M.R., Lu, M., Luo, Y., Ma, Y., Myneni, R.B., Poulter, B., Sun, Z., Wang, T., Viovy, N., Zaehle, S., Zeng, N.: Evaluation of terrestrial carbon cycle models for their response to climate variability and to CO_2 trends, Global Change Biol., 19, 2117-2132, doi:10.1111/gcb.12187, 2013.

Pierce, D.W., Westerling, A.L., Oyler, J.: Future humidity trends over the western United States in the CMIP5 global climate models and variable infiltration capacity hydrological modeling system, Hydrol. Earth Syst. Sci., 17, 1833-1850, doi:10.5194/hess-17-1833-2013, 2013.

Potter, C.S., Randerson, J.T., Field, C.B., Matson, P.A., Vitousek, P.M., Mooney, H.A., Klooster, S.A.: Terrestrial ecosystem production: A process model-based on global satellite and surface data, Global Biogeochem. Cycles, 7, 811-841, doi:10.1029/93gb02725, 1993.

Prentice, I.C., Dong, N., Gleason, S.M., Maire, V., Wright, I.J.: Balancing the costs of carbon gain and water transport: testing a new theoretical framework for plant functional ecology, Ecol. Lett., 17, 82-91, doi:10.1111/ele.12211, 2014.

Rawson, H.M., Begg, J.E., Woodward, R.G.: The effect of atmospheric humidity on photosynthesis, transpiration and water use efficiency of leaves of several plant species, Planta, 134, 5-10, doi:10.1007/bf00390086, 1977.

Reichstein, M., Falge, E., Baldocchi, D., Papale, D., Aubinet, M., Berbigier, P., Bernhofer, C., Buchmann, N., Gilmanov, T., Granier, A., Grunwald, T., Havrankova, K., Ilvesniemi, H., Janous, D., Knohl, A., Laurila, T., Lohila, A., Loustau, D., Matteucci, G., Meyers, T., Miglietta, F., Ourcival, J.-M., Pumpanen, J., Rambal, S., Rotenberg, E., Sanz, M., Tenhunen, J., Seufert, G., Vaccari, F., Vesala, T., Yakir, D., Valentini, R.: On the separation of net ecosystem exchange into assimilation and ecosystem respiration: review and improved algorithm, Global Change Biol., 11, 1424-1439, doi:10.1111/j.1365-2486.2005.001002.x, 2005.

Rienecker, M.M., Suarez, M.J., Gelaro, R., Todling, R., Bacmeister, J., Liu, E., Bosilovich, M.G., Schubert, S.D., Takacs, L., Kim, G.-K., Bloom, S., Chen, J., Collins, D., Conaty, A., Da Silva, A., Gu, W., Joiner, J., Koster, R.D., Lucchesi, R., Molod, A., Owens, T., Pawson, S., Pegion, P., Redder, C.R., Reichle, R., Robertson, F.R., Ruddick, A.G., Sienkiewicz, M., Woollen, J.: MERRA: NASA's modern-era retrospective analysis for research and applications, J. Clim., 24, 3624-3648, doi:10.1175/jcli-d-11-00015.1, 2011.

Running, S.W., Nemani, R.R., Heinsch, F.A., Zhao, M.S., Reeves, M., Hashimoto, H.: A continuous satellite-derived measure of global terrestrial primary production, Bioscience, 54, 547-560, doi:10.1641/0006-3568(2004)054[0547:acsmog]2.0.co;2, 2004.

Ryu, Y., Baldocchi, D.D., Kobayashi, H., van Ingen, C., Li, J., Black, T.A., Beringer, J., van Gorsel, E., Knohl, A., Law, B.E., Roupsard, O.: Integration of MODIS land and atmosphere products with a coupled-process model to estimate gross

primary productivity and evapotranspiration from 1 km to global scales, Global Biogeochem. Cycles, 2510.1029/2011gb004053, 2011.

Ryu, Y., Berry, J.A., Baldocchi, D.D.: What is global photosynthesis? History, uncertainties and opportunities, Remote Sens. Environ., 223, 95-114, doi:10.1016/j.rse.2019.01.016, 2019.

Saleska, S.R., Didan, K., Huete, A.R., da Rocha, H.R.: Amazon forests green-up during 2005 drought, Science, 318, 612-612, doi:10.1126/science.1146663, 2007.

Samanta, A., Ganguly, S., Hashimoto, H., Devadiga, S., Vermote, E., Knyazikhin, Y., Nemani, R.R., Myneni, R.B.: Amazon forests did not green-up during the 2005 drought, Geophys. Res. Lett., 3710.1029/2009gl042154, 2010.

Serbin, S.P., Dillaway, D.N., Kruger, E.L., Townsend, P.A.: Leaf optical properties reflect variation in photosynthetic metabolism and its sensitivity to temperature, J. Exp. Bot., 63, 489-502, doi:10.1093/jxb/err294, 2012.

Simmons, A.J., Willett, K.M., Jones, P.D., Thorne, P.W., Dee, D.P.: Low-frequency variations in surface atmospheric humidity, temperature, and precipitation: Inferences from reanalyses and monthly gridded observational data sets, J. Geophys. Res. D: Atmos., 11510.1029/2009jd012442, 2010.

Sjostrom, M., Zhao, M., Archibald, S., Arneth, A., Cappelaere, B., Falk, U., de Grandcourt, A., Hanan, N., Kergoat, L., Kutsch, W., Merbold, L., Mougin, E., Nickless, A., Nouvellon, Y., Scholes, R.J., Veenendaal, E.M., Ardo, J.: Evaluation of MODIS gross primary productivity for Africa using eddy covariance data, Remote Sens. Environ., 131, 275-286, doi:10.1016/j.rse.2012.12.023, 2013.

Smith, W.K., Reed, S.C., Cleveland, C.C., Ballantyne, A.P., Anderegg, W.R.L., Wieder, W.R., Liu, Y.Y., Running, S.W.: Large divergence of satellite and Earth system model estimates of global terrestrial CO_2 fertilization, Nat. Clim. Change, 6, 306-310, doi:10.1038/nclimate2879, 2016.

Stocker, B.D., Zscheischler, J., Keenan, T.F., Prentice, I.C., Seneviratne, S.I., Peñuelas, J.: Drought impacts on terrestrial primary production underestimated by satellite monitoring, Nat. Geosci., 12, 264-270, doi:10.1038/s41561-019-0318-6, 2019.

Sulman, B.N., Roman, D.T., Yi, K., Wang, L., Phillips, R.P., Novick, K.A.: High atmospheric demand for water can limit forest carbon uptake and transpiration as severely as dry soil, Geophys. Res. Lett., 43, 9686-9695, doi:10.1002/2016gl069416, 2016.

Tan, B., Woodcock, C.E., Hu, J., Zhang, P., Ozdogan, M., Huang, D., Yang, W., Knyazikhin, Y., Myneni, R.B.: The impact of gridding artifacts on the local spatial properties of MODIS data: Implications for validation, compositing, and band-to-band registration across resolutions, Remote Sens. Environ., 105, 98-114, doi:10.1016/j.rse.2006.06.008, 2006.

Tang, S., Chen, J.M., Zhu, Q., Li, X., Chen, M., Sun, R., Zhou, Y., Deng, F., Xie, D.: LAI inversion algorithm based on directional reflectance kernels, J. Environ. Manage., 85, 638-648, doi:10.1016/j.jenvman.2006.08.018, 2007.

Urban, O., Janous, D., Acosta, M., Czerny, R., Markova, I., Navratil, M., Pavelka, M., Pokorny, R., Sprtova, M., Zhang, R., Spunda, V., Grace, J., Marek, M.V.: Ecophysiological controls over the net ecosystem exchange of mountain spruce stand.

Comparison of the response in direct vs. diffuse solar radiation, Global Change Biol., 13, 157-168, doi:10.1111/j.1365-2486.2006.01265.x, 2007.

Van Wijngaarden, W.A., Vincent, L.A.: Trends in relative humidity in Canada from 1953–2003. In 15th Symp. on Global Change and Climate Variations, 2004.

Vuichard, N., Papale, D.: Filling the gaps in meteorological continuous data measured at FLUXNET sites with ERA-Interim reanalysis, Earth Syst. Sci. Data, 7, 157-171, doi:10.5194/essd-7-157-2015, 2015.

Wang, Z., Skidmore, A.K., Darvishzadeh, R., Wang, T.: Mapping forest canopy nitrogen content by inversion of coupled leaf-canopy radiative transfer models from airborne hyperspectral imagery, Agric. For. Meteorol., 253, 247-260, doi:10.1016/j.agrformet.2018.02.010, 2018.

Wild, M., Gilgen, H., Roesch, A., Ohmura, A., Long, C.N., Dutton, E.G., Forgan, B., Kallis, A., Russak, V., Tsvetkov, A.: From dimming to brightening: Decadal changes in solar radiation at Earth's surface, Science, 308, 847-850, doi:10.1126/science.1103215, 2005.

Willett, K.M., Dunn, R.J.H., Thorne, P.W., Bell, S., de Podesta, M., Parker, D.E., Jones, P.D., Williams, C.N., Jr.: HadISDH land surface multi-variable humidity and temperature record for climate monitoring, Climate of the Past, 10, 1983-2006, doi:10.5194/cp-10-1983-2014, 2014.

Williams, A.P., Allen, C.D., Macalady, A.K., Griffin, D., Woodhouse, C.A., Meko, D.M., Swetnam, T.W., Rauscher, S.A., Seager, R., Grissino-Mayer, H.D., Dean, J.S., Cook, E.R., Gangodagamage, C., Cai, M., McDowell, N.G.: Temperature as a potent driver of regional forest drought stress and tree mortality, Nat. Clim. Change, 3, 292-297, doi:10.1038/nclimate1693, 2013.

Wu, J., Albert, L.P., Lopes, A.P., Restrepo-Coupe, N., Hayek, M., Wiedemann, K.T., Guan, K., Stark, S.C., Christoffersen, B., Prohaska, N., Tavares, J.V., Marostica, S., Kobayashi, H., Ferreira, M.L., Campos, K.S., da Silva, R., Brando, P.M., Dye, D.G., Huxman, T.E., Huete, A.R., Nelson, B.W., Saleska, S.R.: Leaf development and demography explain photosynthetic seasonality in Amazon evergreen forests, Science, 351, 972-976, doi:10.1126/science.aad5068, 2016.

Wu, J., Guan, K., Hayek, M., Restrepo-Coupe, N., Wiedemann, K.T., Xu, X., Wehr, R., Christoffersen, B.O., Miao, G., da Silva, R., de Araujo, A.C., Oliviera, R.C., Camargo, P.B., Monson, R.K., Huete, A.R., Saleska, S.R.: Partitioning controls on Amazon forest photosynthesis between environmental and biotic factors at hourly to interannual timescales, Global Change Biol., 23, 1240-1257, doi:10.1111/gcb.13509, 2017.

Xiao, X.M., Zhang, Q.Y., Hollinger, D., Aber, J., Moore, B.: Modeling gross primary production of an evergreen needleleaf forest using MODIS and climate data, Ecol. Appl., 15, 954-969, doi:10.1890/04-0470, 2005.

Xiao, Z., Liang, S., Wang, J., Xiang, Y., Zhao, X., Song, J.: Long-Time-Series Global Land Surface Satellite Leaf Area Index Product Derived From MODIS and AVHRR Surface Reflectance, IEEE Trans. Geosci. Remote Sens., 54, 5301-5318, doi:10.1109/tgrs.2016.2560522, 2016.

Xu, B., Li, J., Park, T., Liu, Q., Zeng, Y., Yin, G., Zhao, J., Fan, W., Yang, L., Knyazikhin, Y., Myneni, R.B.: An integrated method for validating long-term leaf area index products using global networks of site-based measurements, Remote Sens. Environ., 209, 134-151, doi:10.1016/j.rse.2018.02.049, 2018.

Yoder, B.J., Pettigrew-Crosby, R.E.: Predicting nitrogen and chlorophyll content and concentrations from reflectance spectra (400-2500 nm) at leaf and canopy scales, Remote Sens. Environ., 53, 199-211, doi:10.1016/0034-4257(95)00135-n, 1995.

Yuan, W., Cai, W., Xia, J., Chen, J., Liu, S., Dong, W., Merbold, L., Law, B., Arain, A., Beringer, J., Bernhofer, C., Black, A., Blanken, P.D., Cescatti, A., Chen, Y., Francois, L., Gianelle, D., Janssens, I.A., Jung, M., Kato, T., Kiely, G., Liu, D., Marcolla, B., Montagnani, L., Raschi, A., Roupsard, O., Varlagin, A., Wohlfahrt, G.: Global comparison of light use efficiency models for simulating terrestrial vegetation gross primary production based on the La Thuile database, Agric. For. Meteorol., 192, 108-120, doi:10.1016/j.agrformet.2014.03.007, 2014.

Yuan, W., Liu, S., Zhou, G., Zhou, G., Tieszen, L.L., Baldocchi, D., Bernhofer, C., Gholz, H., Goldstein, A.H., Goulden, M.L., Hollinger, D.Y., Hu, Y., Law, B.E., Stoy, P.C., Vesala, T., Wofsy, S.C., AmeriFlux, C.: Deriving a light use efficiency model from eddy covariance flux data for predicting daily gross primary production across biomes, Agric. For. Meteorol., 143, 189-207, doi:10.1016/j.agrformet.2006.12.001, 2007.

Yuan, W., Luo, Y., Li, X., Liu, S., Yu, G., Zhou, T., Bahn, M., Black, A., Desai, A.R., Cescatti, A., Marcolla, B., Jacobs, C., Chen, J., Aurela, M., Bernhofer, C., Gielen, B., Bohrer, G., Cook, D.R., Dragoni, D., Dunn, A.L., Gianelle, D., Gruenwald, T., Ibrom, A., Leclerc, M.Y., Lindroth, A., Liu, H., Marchesini, L.B., Montagnani, L., Pita, G., Rodeghiero, M., Rodrigues, A., Starr, G., Stoy, P.C.: Redefinition and global estimation of basal ecosystem respiration rate, Global Biogeochem. Cycles, 2510.1029/2011gb004150, 2011.

Yuan, W., Liu, S., Yu, G., Bonnefond, J.-M., Chen, J., Davis, K., Desai, A.R., Goldstein, A.H., Gianelle, D., Rossi, F., Suyker, A.E., Verma, S.B.: Global estimates of evapotranspiration and gross primary production based on MODIS and global meteorology data, Remote Sens. Environ., 114, 1416-1431, doi:10.1016/j.rse.2010.01.022, 2010.

Yuan, W., Zheng, Y., Piao, S., Ciais, P., Lombardozzi, D., Wang, Y., Ryu, Y., Chen, G., Dong, W., Hu, Z., Jain, A.K., Jiang, C., Kato, E., Li, S., Lienert, S., Liu, S., Nabel, J.E.M.S., Qin, Z., Quine, T., Sitch, S., Smith, W.K., Wang, F., Wu, C., Xiao, Z., Yang, S.: Increased atmospheric vapor pressure deficit reduces global vegetation growth, Science Advances, 510.1126/sciadv.aax1396, 2019.

Zhang, Y., Xiao, X., Wu, X., Zhou, S., Zhang, G., Qin, Y., Dong, J.: Data Descriptor: A global moderate resolution dataset of gross primary production of vegetation for 2000-2016, Scientific Data, 410.1038/sdata.2017.165, 2017.

Zhao, M., Running, S.W.: Drought-Induced Reduction in Global Terrestrial Net Primary Production from 2000 Through 2009, Science, 329, 940-943, doi:10.1126/science.1192666, 2010.

Zheng, Y., Shen, R.; Wang, Y., Li, X., Liu, S., Liang, S., Chen, Jing M., Ju, W., Zhang, L., Yuan, W.: Improved estimate of global gross primary production for reproducing its long-term variation, 1982-2017. figshare. Dataset. doi:10.6084/m9.figshare.8942336, 2019.

Zheng, Y., Zhang, L., Xiao, J., Yuan, W., Yan, M., Li, T., Zhang, Z.: Sources of uncertainty in gross primary productivity simulated by light use efficiency models: Model structure, parameters, input data, and spatial resolution, Agric. For. Meteorol., 263, 242-257, doi:10.1016/j.agrformet.2018.08.003, 2018.

Zhu, Z., Piao, S., Myneni, R.B., Huang, M., Zeng, Z., Canadell, J.G., Ciais, P., Sitch, S., Friedlingstein, P., Arneth, A., Cao, C., Cheng, L., Kato, E., Koven, C., Li, Y., Lian, X., Liu, Y., Liu, R., Mao, J., Pan, Y., Peng, S., Penuelas, J., Poulter, B., Pugh, T.A.M., Stocker, B.D., Viovy, N., Wang, X., Wang, Y., Xiao, Z., Yang, H., Zaehle, S., Zeng, N.: Greening of the Earth and its drivers, Nat. Clim. Change, 6, 791-796, doi:10.1038/nclimate3004, 2016.

Tables

Table 1: Information on the eddy covariance (EC) sites used in this study.

Site Name	Latitude	Longitude	Vegetation Type	Study Period
*DE-Kli	50.89ºN	13.52ºE	CRO	2004-2012
DE-RuS	50.87ºN	6.45ºE	CRO	2011-2012
FI-Jok	60.90ºN	23.51ºE	CRO	2001-2003
*FR-Gri	48.84ºN	1.95ºE	CRO	2005-2012
*US-ARM	36.61ºN	97.49ºW	CRO	2003-2012
*US-Ne1	41.16ºN	96.47ºW	CRO	2001-2012
*US-Ne2	41.16ºN	96.47ºW	CRO	2001-2012
*US-Ne3	41.17ºN	96.43ºW	CRO	2001-2012
CA-TPD	42.64ºN	80.56ºW	DBF	2012
*DE-Hai	51.08ºN	10.45ºE	DBF	2000-2012
*DK-Sor	55.49ºN	11.64ºE	DBF	2001-2012
*FR-Fon	48.48ºN	2.78ºE	DBF	2005-2012
IT-PT1	45.20ºN	9.06ºE	DBF	2002-2004
*IT-Ro2	42.39ºN	11.92ºE	DBF	2002-2008; 2010-2012
JP-MBF	44.39ºN	142.32ºE	DBF	2004-2005
*US-Ha1	42.54ºN	72.17ºW	DBF	1992-2012
*US-MMS	39.32ºN	86.41ºW	DBF	1999-2012
*US-Oho	41.55ºN	83.84ºW	DBF	2004-2012
*US-UMB	45.56ºN	84.71ºW	DBF	2000-2012
*US-UMd	45.56ºN	84.70ºW	DBF	2008-2012
*US-WCr	45.81ºN	90.08ºW	DBF	1999-2006; 2011-2012
*BR-Sa1	2.86ºS	54.96ºW	EBF	2002-2005; 2008-2011
BR-Sa3	3.02ºS	54.97ºW	EBF	2001-2003
CN-Din	23.17ºN	112.54ºE	EBF	2003-2005
*FR-Pue	43.74ºN	3.60ºE	EBF	2000-2012
*GF-Guy	5.28ºN	52.92ºW	EBF	2004-2012
*MY-PSO	2.97ºN	102.31ºE	EBF	2003-2009
CA-NS1	55.88ºN	98.48ºW	ENF	2002-2005
*CA-NS2	55.91ºN	98.52ºW	ENF	2001-2005
CA-NS3	55.91ºN	98.38ºW	ENF	2002-2005
CA-NS4	55.91ºN	98.38ºW	ENF	2003-2005
*CA-NS5	55.86ºN	98.49ºW	ENF	2001-2005

*CA-Qfo	49.69ºN	74.34ºW	ENF	2003-2010
CA-SF1	54.49ºN	105.82ºW	ENF	2003-2006
*CA-SF2	54.25ºN	105.88ºW	ENF	2001-2005
*CA-TP1	42.66ºN	80.56ºW	ENF	2003-2012
*CA-TP2	42.77ºN	80.46ºW	ENF	2003-2007
*CA-TP3	42.71ºN	80.35ºW	ENF	2003-2012
CN-Qia	26.74ºN	115.06ºE	ENF	2003-2005
*CZ-BK1	49.50ºN	18.54ºE	ENF	2004-2012
DE-Lkb	49.10ºN	13.30ºE	ENF	2009-2012
*DE-Obe	50.78ºN	13.72ºE	ENF	2008-2012
*DE-Tha	50.96ºN	13.57ºE	ENF	1996-2012
*FI-Hyy	61.85ºN	24.30ºE	ENF	1996-2012
IT-La2	45.95ºN	11.29ºE	ENF	2001
*IT-Lav	45.96ºN	11.28ºE	ENF	2003-2012
*IT-Ren	46.59ºN	11.43ºE	ENF	1999-2012
*IT-SRo	43.73ºN	10.28ºE	ENF	2001-2012
*NL-Loo	52.17ºN	5.74ºE	ENF	1996-2012
*RU-Fyo	56.46ºN	32.92ºE	ENF	1998-2012
*US-Blo	38.90ºN	120.63ºW	ENF	1997-2007
*US-Me2	44.45ºN	121.56ºW	ENF	2002-2012
US-Me6	44.32ºN	121.61ºW	ENF	2011-2012
*US-NR1	40.03ºN	105.55ºW	ENF	1999-2012
*CH-Cha	47.21ºN	8.41ºE	GRA	2006-2008; 2010-2012
*CH-Fru	47.12ºN	8.54ºE	GRA	2006-2008; 2010-2012
*CH-Oe1	47.29ºN	7.73ºE	GRA	2002-2008
CN-Cng	44.59ºN	123.51ºE	GRA	2007-2010
CN-Du2	42.05ºN	116.28ºE	GRA	2007-2008
CN-HaM	37.37ºN	101.18ºE	GRA	2002-2003
*CZ-BK2	49.49ºN	18.54ºE	GRA	2006-2011
*NL-Hor	52.24ºN	5.07ºE	GRA	2004-2011
RU-Ha1	54.73ºN	90.00ºE	GRA	2002-2004
US-AR1	36.43ºN	99.42ºW	GRA	2009-2012
US-AR2	36.64ºN	99.60ºW	GRA	2009-2012
*US-Goo	34.25ºN	89.87ºW	GRA	2002-2006
*US-IB2	41.84ºN	88.24ºW	GRA	2005; 2007-2011
*BE-Bra	51.31ºN	4.52ºE	MF	1999-2002; 2004-2012
*BE-Vie	50.31ºN	6.00ºE	MF	1997-2012

*CA-Gro	48.22ºN	82.16ºW	MF	2004-2012
CN-Cha	42.40ºN	128.10ºE	MF	2003-2005
JP-SMF	35.26ºN	137.08ºE	MF	2003-2006
*US-PFa	45.95ºN	90.27ºW	MF	1996-2012
*US-Syv	46.24ºN	89.35ºW	MF	2001-2006; 2012
AU-Ade	13.08ºS	131.12ºE	SAV	2007-2009
AU-Cpr	34.00ºS	140.59ºE	SAV	2011-2012
*AU-DaS	14.16ºS	131.39ºE	SAV	2008-2012
AU-Dry	15.26ºS	132.37ºE	SAV	2009-2012
AU-RDF	14.56ºS	132.48ºE	SAV	2011-2012
SD-Dem	13.28ºN	30.48ºE	SAV	2007-2009
*US-Ton	38.43ºN	120.97ºW	SAV	2001-2012
ZA-Kru	25.02ºS	31.50ºE	SAV	2009-2012
CA-NS6	55.92ºN	98.96ºW	SRH	2002-2005
CA-NS7	56.64ºN	99.95ºW	SRH	2003-2005
*CA-SF3	54.09ºN	106.01ºW	SRH	2002-2006
ES-LgS	37.10ºN	2.97ºW	SRH	2007-2009
US-KS2	28.61ºN	80.67ºW	SRH	2003-2006
CN-Ha2	37.61ºN	101.33ºE	WET	2003-2005
DE-Akm	53.87ºN	13.68ºE	WET	2010-2012
DE-SfN	47.81ºN	11.33ºE	WET	2012
DE-Spw	51.89ºN	14.03ºE	WET	2010-2012
RU-Che	68.61ºN	161.34ºE	WET	2002-2004
US-Ivo	68.49ºN	155.75ºW	WET	2004-2007
*US-Los	46.08ºN	89.98ºW	WET	2001-2008; 2010
US-WPT	41.46ºN	83.00ºW	WET	2011-2012

* indicates the site used to investigate the interannual variations in GPP with observations greater than 5-years.

Table 2: Input datasets used to drive the revised EC-LUE model.

Variable	Dataset/provider	Source
Air temperature	MERRA2	https://gmao.gsfc.nasa.gov/reanalysis/MERRA-2/
Dew point temperature	MERRA2	https://gmao.gsfc.nasa.gov/reanalysis/MERRA-2/
Direct PAR	MERRA2	https://gmao.gsfc.nasa.gov/reanalysis/MERRA-2/
Diffuse PAR	MERRA2	https://gmao.gsfc.nasa.gov/reanalysis/MERRA-2/
LAI	GLASS	http://www.glass.umd.edu/Download.html
Landcover map	MCD12Q1	https://lpdaac.usgs.gov/products/mcd12q1v006/
C4 crop percentage	ISLSCP II C4 Vegetation Percentage	https://doi.org/10.3334/ORNLDAAC/932
CO_2 concentration	NOAA's Earth System Research Laboratory	www.esrl.noaa.gov/gmd/ccgg/trends/

680

Table 3: Optimized parameters (ε_{msu}, ε_{msh}, φ, and VPD_0) of the revised EC-LUE model for different vegetation types.

Vegetation Types	DBF	ENF	EBF	MF	GRA	CRO-C3	CRO-C4	SAV	SHR	WET
ε_{msu} (g C MJ^{-1})	1.28 ±0.36	1.72 ±0.42	1.67 ±0.85	1.38 ±0.21	1.16 ±0.15	1.25 ±0.42	2.46 ±0.78	2.24 ±0.68	1.21 ±0.25	1.34 ±0.26
ε_{msh} (g C MJ^{-1})	3.59 ±0.66	3.87 ±0.58	4.35 ±0.72	3.29 ±0.63	1.91 ±0.46	2.46 ±0.52	5.64 ±1.02	4.26 ±0.95	2.71 ±0.52	2.62 ±0.49
φ (ppm)	32 ±8.25	25 ±7.59	20 ±6.36	49 ±11.25	57 ±11.85	43 ±9.56	54 ±15.36	54 ±12.23	34 ±7.59	36 ±10.32
VPD_0 (k Pa)	1.15 ±0.25	1.34 ±0.26	0.57 ±0.15	0.62 ±0.14	1.69 ±0.35	1.02 ±0.19	1.53 ±0.31	1.65 ±0.26	1.34 ±0.21	0.62 ±0.12

Figures

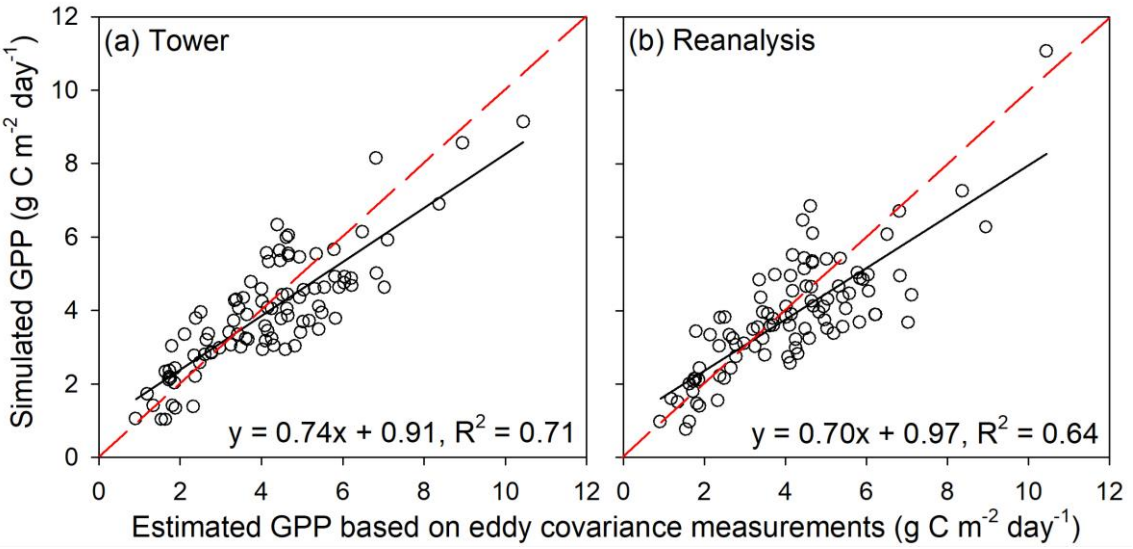

Figure 1: Comparisons between annual mean GPP estimated from EC towers and annual mean GPP simulated by the revised EC-LUE model. The modeled GPP were simulated using (a) tower-derived meteorology and (b) global reanalysis meteorology. The black lines are the regression lines, and the red dash lines are the 1:1 lines. The insert equations are the regression equations derived from all the sites.

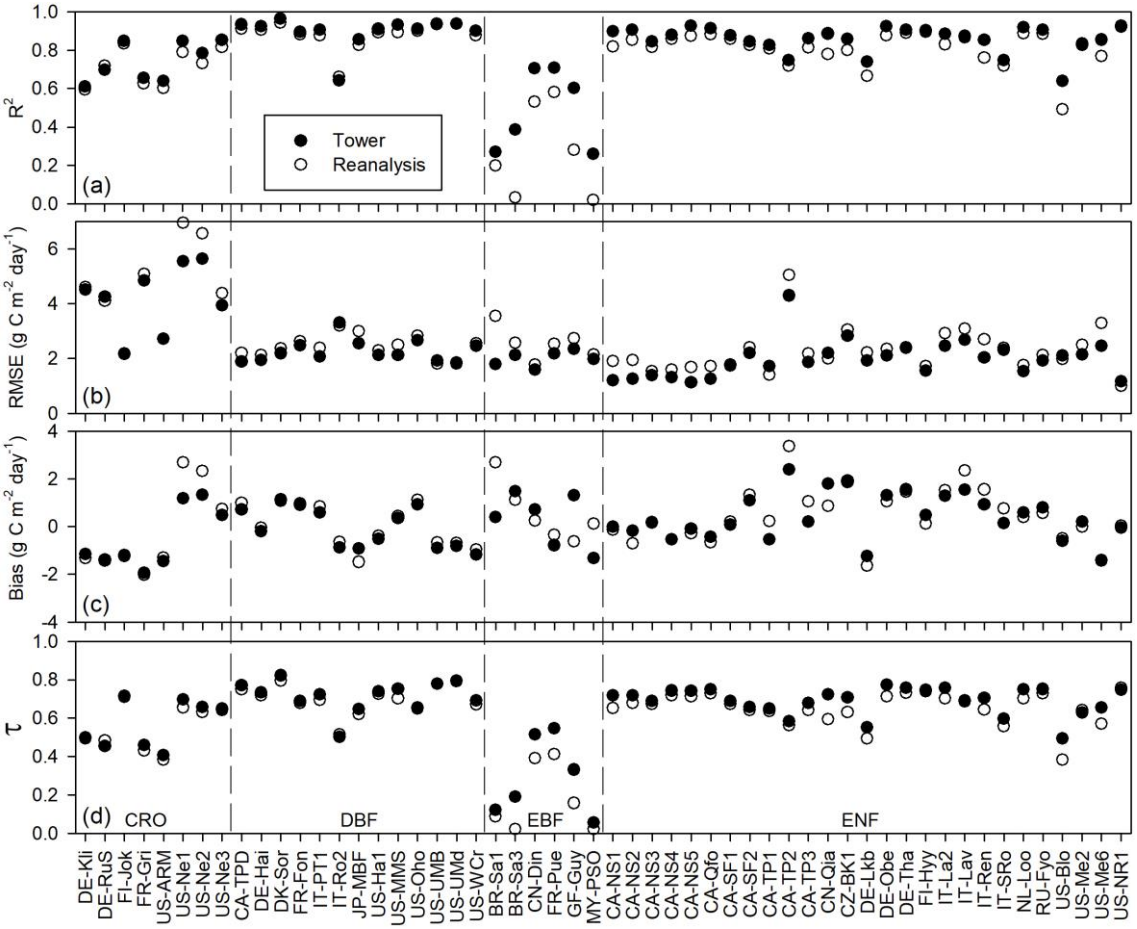

Figure 2: Comparisons of 8-day mean GPP between the model simulated GPP and tower estimated GPP. Solid and open dots indicate the GPP simulations derived from tower-derived meteorology data and meteorological reanalysis dataset, respectively.

695

Figure 2 (continue)

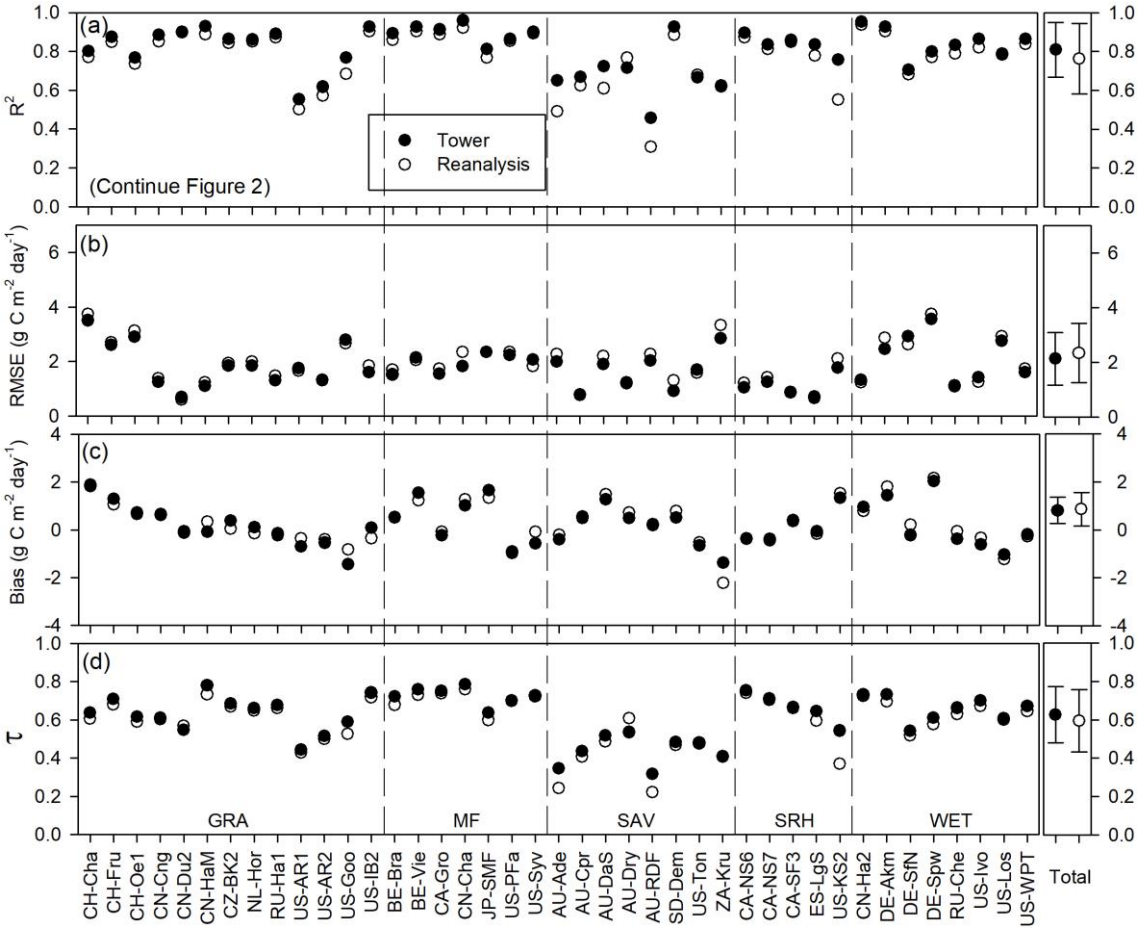

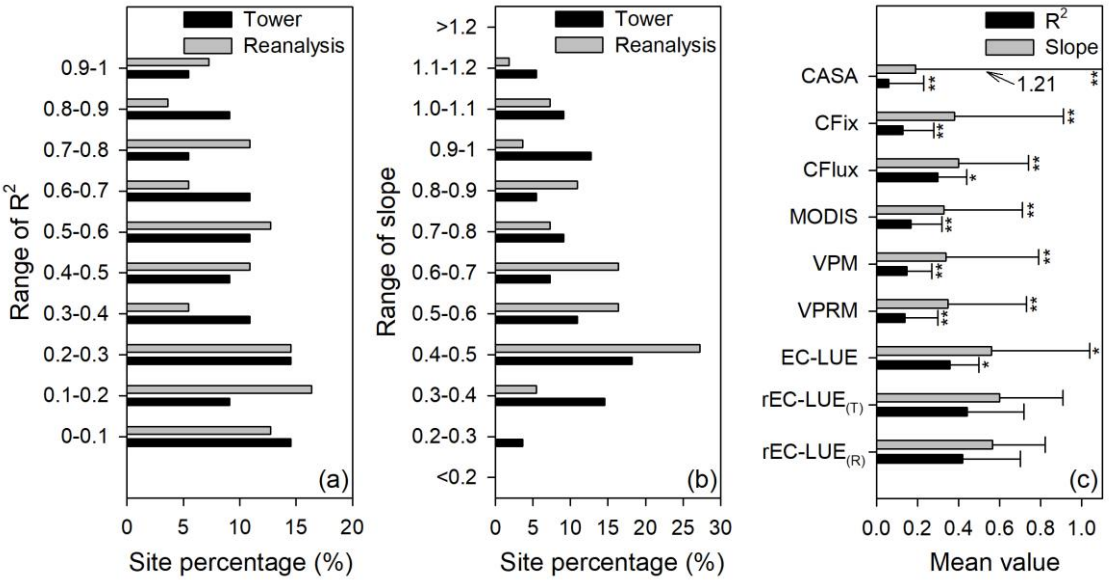

Figure 3: Site percentage of (a) correlation coefficients (R^2), and (b) regression slopes between the model simulated and tower-based interannual variabilities in GPP. (c) Averaged values (error bars represent the standard deviations) of R^2 and slope for various LUE models. rEC-LUE$_{(T)}$ and rEC-LUE$_{(R)}$ indicate the revised EC-LUE models derived from tower-derived meteorology data and meteorological reanalysis dataset. The R^2 and slopes of the other seven LUE models (i.e., EC-LUE, VPRM, VPM, MODIS, CFlux, CFix, and CASA) in the figure were obtained from the study by Yuan et al. (2014). ** and * indicate a significant difference in statistic variables (R^2 and slope) between the rEC-LUE$_{(T)}$ and other LUE models (i.e., rEC-LUE$_{(T)}$ and other seven LUE models) at p-value < 0.01 and p-value<0.05, respectively.

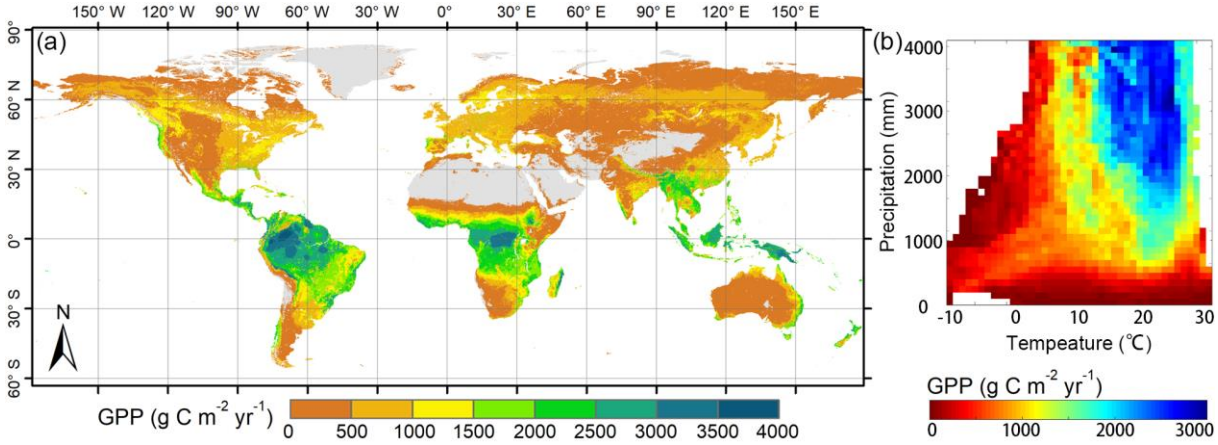

Figure 4: Spatial pattern of global GPP simulated by the revised EC-LUE model during 1982–2017: (a) averaged annual GPP, (b) averaged annual GPP at different temperature and precipitation gradients.

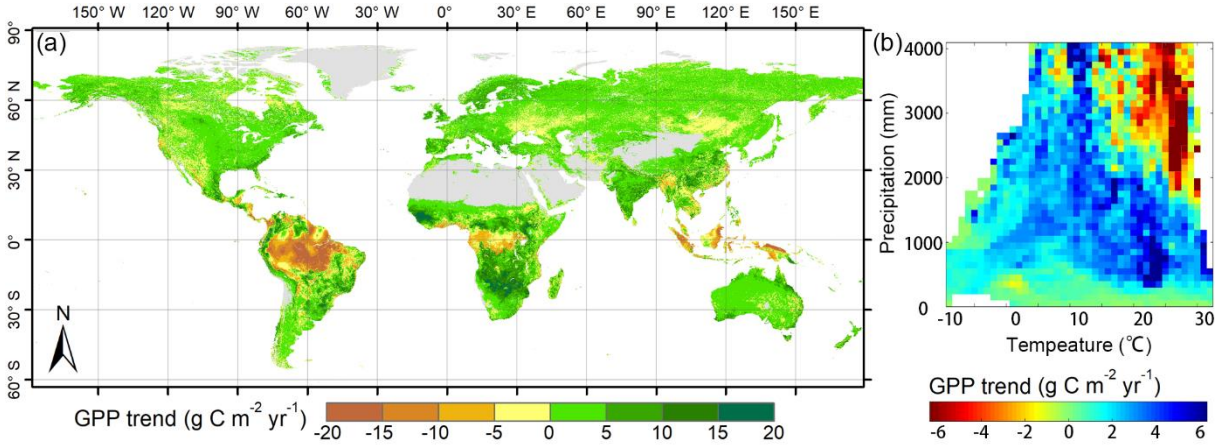

Figure 5: Spatial pattern of global GPP trend simulated by the revised EC-LUE models during 1982–2017: (a) trend of annual GPP, (b) trend of annual GPP at different temperature and precipitation gradients.

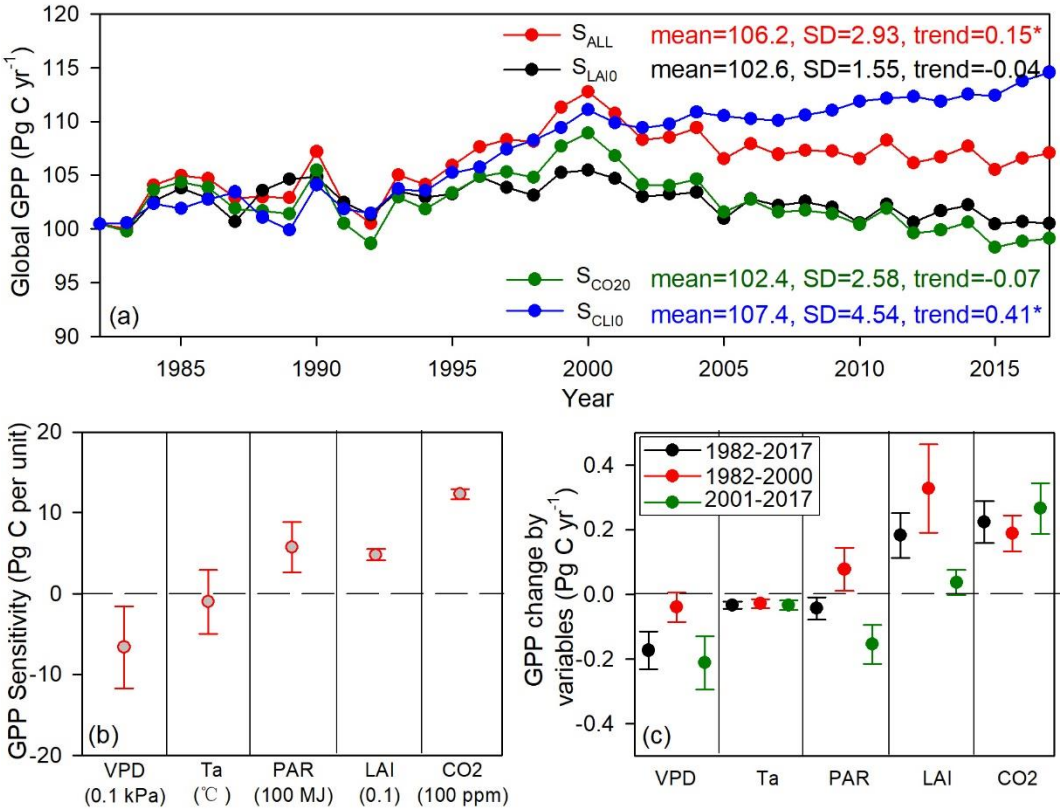

Figure 6: Long-term changes in global GPP and the environmental regulations: (a) Global summed GPP derived from the four experimental simulations in section 2.5, (b) GPP sensitivity to climate variables (i.e., VPD, Ta, and PAR), LAI, and atmospheric CO_2, (c) contributions of climate variables (i.e., VPD, Ta, and PAR), LAI, and atmospheric CO_2 to GPP changes over 1982–2017, 1982–2000, and 2001–2017. * indicates the significant level at *p*-value<0.05.

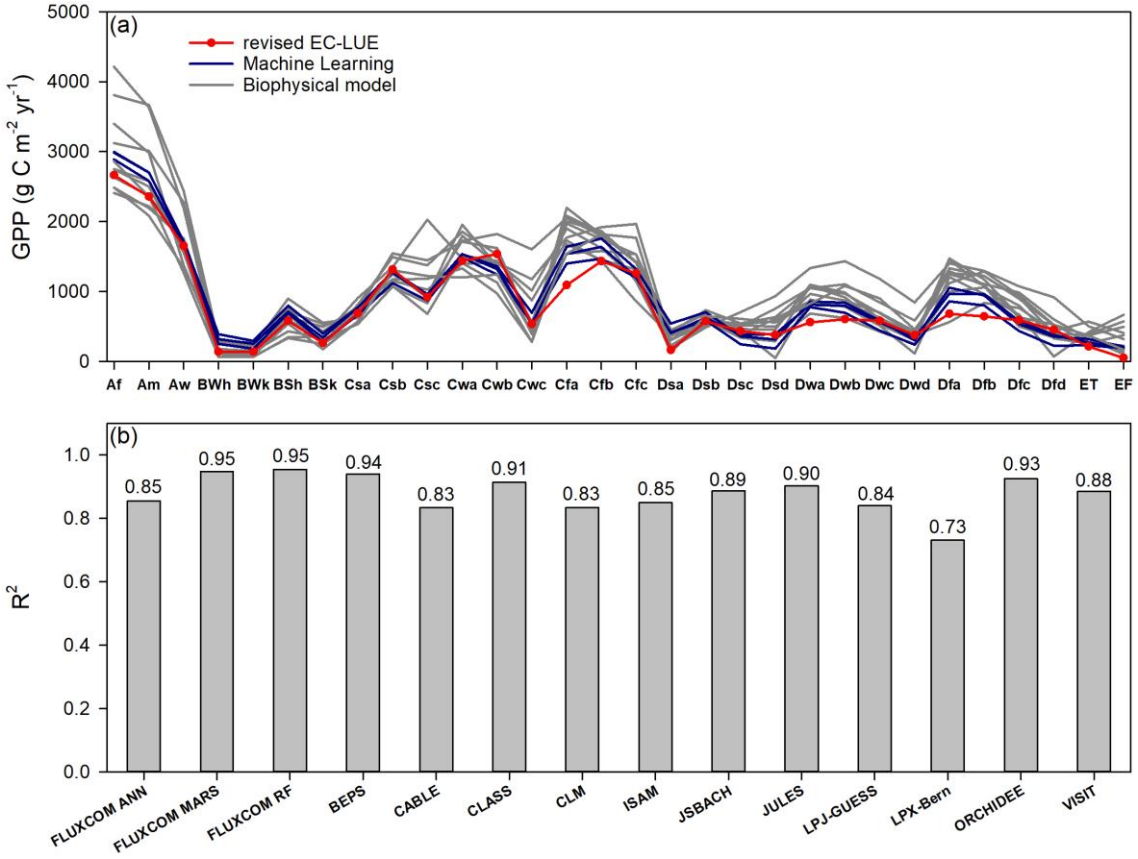

Figure 7: Comparisons of long-term (1982 to 2010s) averaged GPP between the revised EC-LUE model and other models across bioclimatic zones in the Köppen-Geiger climate classification map (Beck et al., 2018). (a) the regional averaged value (b) correlation coefficients (R^2) of GPP across all the bioclimatic zones between the revised EC-LUE model and other models. These models including machine learning models (FLUXCOM ANN, FLUXCOM MARS, FLUXCOM RF; Jung et al., 2017), biophysical models BEPS (Ju et al., 2006; Liu et al., 2018), and ten biophysical models in TRENDY (CABLE, CLASS, CLM, ISAM, JSBACH, JULES, LPJ-GUESS, LPX-Bern, ORCHIDEE, and VISIT). The abbreviations for the bioclimatic zones are as follows: Af, tropical, rainforest; Am, tropical, monsoon; Aw, tropical, savannah; BWh, arid, desert, hot; BWk, arid, desert, cold; BSh, arid, steppe, hot; BSk, arid, steppe, cold; Csa, temperate, dry summer, hot summer; Csb, temperate, dry summer, warm summer; Csc, temperate, dry summer, cold summer; Cwa, temperate, dry winter, hot summer; Cwb, temperate, dry winter, warm summer; Cwc, temperate, dry winter, cold summer; Cfa, temperate, no dry season, hot summer; Cfb temperate, no dry season, warm summer; Cfc, temperate, no dry season, cold summer; Dsa, cold, dry summer, hot summer; Dsb, cold, dry summer, warm summer; Dsc, cold, dry summer, cold summer; Dsd, cold, dry summer, very cold winter; Dwa, cold, dry winter, hot summer; Dwb, cold, dry winter, warm summer; Dwc, cold, dry winter, cold summer; Dwd, cold, dry winter, very cold winter; Dfa, cold, no dry season, hot summer; Dfb, cold, no dry season, warm summer; Dfc, cold, no dry season, cold summer; Dfd, cold, no dry season, very cold winter; ET, polar, tundra; EF, polar, frost.

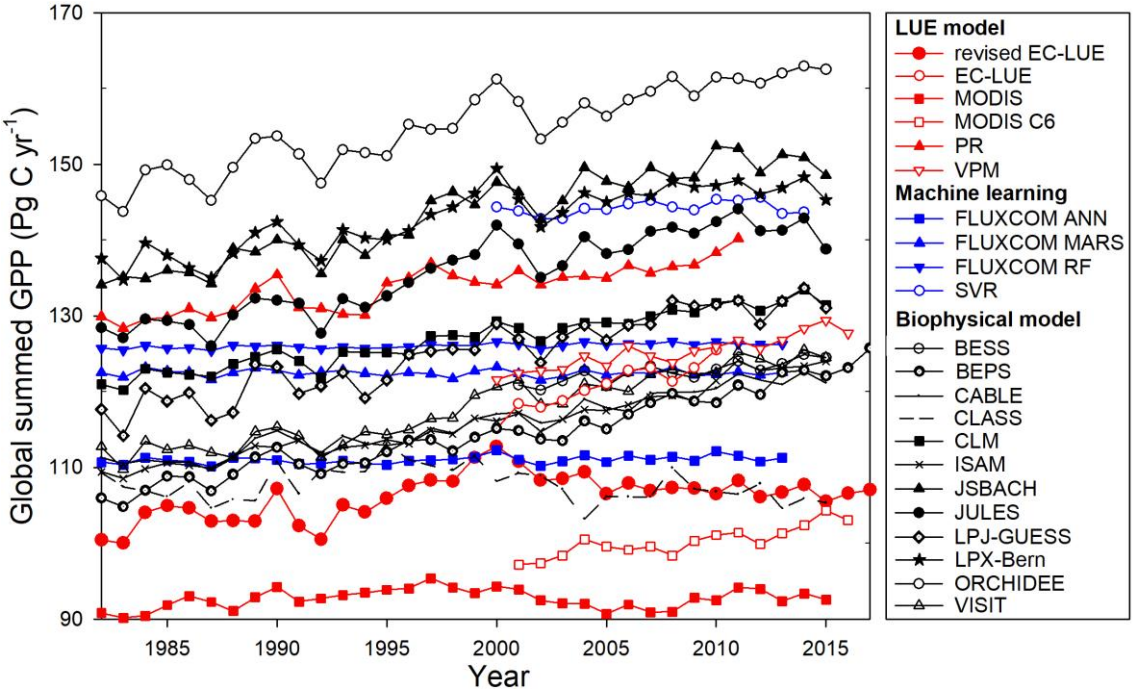

Figure 8: Comparisons of annual global summed GPP estimates from various models. The datasets or model algorithms were obtained from: EC-LUE (Cai et al., 2014), MODIS (Smith et al., 2016), MOD17 C6 (Running et al., 2004), PR (Keenan et al., 2016), VPM (Zhang et al., 2017), FLUXCOM (Jung et al., 2017), SVR (Kondo et al., 2015), BESS (Jiang and Ryu, 2016), BEPS (Ju et al., 2006; Liu et al., 2018), and models in TRENDY (CABLE, CLASS, CLM, ISAM, JSBACH, JULES, LPJ-GUESS, LPX-Bern, ORCHIDEE, and VISIT).

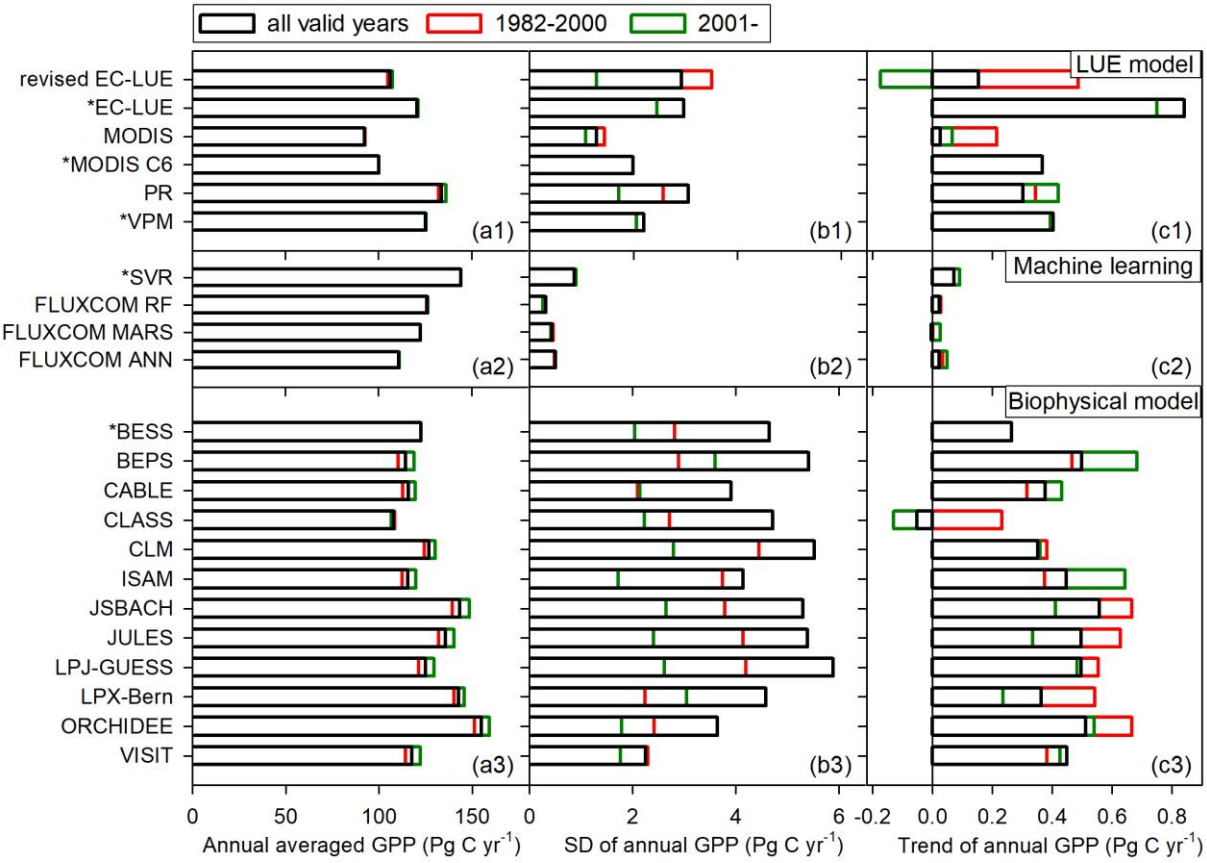

750 **Figure 9: Comparison of (a1)–(a3) averaged annual GPP, (b1)–(b3) interannual variability in annual GPP represented by standard deviation (SD), and (c1)–(c3) annual GPP trend among different GPP datasets or models. The references of these models are the same as in Figure 9. * indicates that the valid period of the dataset begins from 2000 or 2001.**